NUREG/CR-1355
BNL-NUREG-51151

CONAN: AN LMFBR CONTAINMENT RESPONSE COMPUTER CODE

R.D. GASSER

November 1979

ENGINEERING AND ADVANCED REACTOR SAFETY DIVISION
DEPARTMENT OF NUCLEAR ENERGY, BROOKHAVEN NATIONAL LABORATORY
UPTON, NEW YORK 11973

Prepared for
U.S. Nuclear Regulatory Commission
Contract No. DE-AC02-76CH00016

NUREG/CR-1355
BNL-NUREG-51151
R-7

CONAN: AN LMFBR CONTAINMENT RESPONSE COMPUTER CODE

R.D. GASSER

November 1979

ENGINEERING AND ADVANCED REACTOR SAFETY DIVISION
DEPARTMENT OF NUCLEAR ENERGY, BROOKHAVEN NATIONAL LABORATORY
UPTON, NEW YORK 11973

Prepared for
U.S. NUCLEAR REGULATORY COMMISSION
WASHINGTON, D.C. 20555
UNDER INTERAGENCY AGREEMENT DE-AC02-76CH00016
NRC FIN NO. A-3000

ABSTRACT

A description is given for the mathematical models used in the CONAN containment analysis code. The code was designed to study the particular phenomena which are important and limiting in the response of a LMFBR containment system to a hypothetical core melt-through accident. Results obtained using the CONAN code are compared to the exact solution for an adiabatic system and to results obtained from the CACECO containment code. The conclusion drawn from results obtained with CONAN is that the processes of evaporation and condensation, which are not treated mechanistically in the CACECO code, do have a significant effect on the transient and tend to strongly limit the severity of the accident in terms of containment pressurization.

TABLE OF CONTENTS

		Page
ABSTRACT		iii
LIST OF FIGURES		v
I.	INTRODUCTION	1
II.	AN ADIABATIC ENERGY-MASS BALANCE MODEL	2
III.	COMPARISON OF ADIABATIC MODEL BETWEEN CACECO AND CONAN	6
IV.	FORMULATION AND DESCRIPTION OF THE CONAN CODE MODELING	8
V.	RESULTS AND COMPARISONS	15
VI.	CONDENSATION AND EVAPORATION MODELS	25
VII.	EFFECTS OF CONDENSATION AND EVAPORATION	34
VIII.	CONCLUSIONS AND PROJECTIONS FOR FURTHER ANALYSIS	38
REFERENCES		42
NOMENCLATURE		43

LIST OF FIGURES

Figure	Title	Page
1	Adiabatic Two Cell Model.	3
2	Comparison of CACECO Pressures with Exact Solution for Adiabatic System.	7
3	Comparison of CACECO Temperatures with Exact Solution for Adiabatic System.	7
4	Comparison of CONAN Temperatures with Exact Solution for Adiabatic System.	9
5	Comparison of CONAN Pressures with Exact Solution for Adiabatic System.	9
6	CONAN Temperatures for Case 2.	17
7	Comparison of Sodium Pool Temperatures for Case 2.	17
8	Comparison of Cell 1 Atmospheric Temperature for Case 2.	19
9	Comparison of Cell 2 Pressure for Case 2.	19
10	Comparison of Cell 2 Temperature for Case 2.	19
11	Comparison of Cell 2 Equipment Temperature for Case 2.	21
12	Comparison of Cell 2 Roof Temperature for Case 2.	21
13	Comparison of Cell 2 Oxygen Inventory for Case 2.	21
14	CONAN Temperature Results for Case 3.	23
15	Comparison of Temperature Results for Case 3.	23
16	Comparison of Pressures for Case 3.	26
17	Comparison of Cell 2 Oxygen Inventory for Case 3.	26
18	Temperature Drop Across the Sodium Film.	30
19	Temperature Drop Across the Sodium Film.	30
20	Ratio of Heat Flux in the Presence of Non-Condensibles to the Heat Flux without Non-Condensibles.	32
21	Effects of Condensation and Evaporation on the RCB Pressure Transient.	36

LIST OF FIGURES (Cont.)

Figure	Title	Page
22	Effects of Condensation on the Cavity Temperatures.	36
23	Condensation versus Evaporation Rates.	39
24	Effects of Condensation and Evaporation on Sodium Vapor Density.	39

I. INTRODUCTION

Experience with the CACECO code at Brookhaven National Laboratory over a period of three years has revealed a number of areas which warrant further examination in connection with physical modeling. These areas have been, for the most part, related to the energy and continuity equations. In this report, a limited evaluation of the CACECO code mass and energy-balance modeling is presented. A more detailed evaluation of the CACECO code with regard to specific problems which have been encountered in operating the code can be found in Reference 1.

It was thought that an evaluation of these aspects of the CACECO code would be facilitated by the availability of a small, less complicated containment analysis code in which the energy and mass balance equations could be handled in a more rigorous manner. Such a small but versatile code could also be used to study in detail those particular phenomena which are deemed to be important or limiting. The result has been the on-going development of the CONAN containment analysis code.

Of particular concern has been the CACECO modeling for heat transfer between the pool and the atmosphere, as well as its treatment of condensation and vaporization. The standard version of the CACECO code (available through the Argonne Code Center) utilizes a model which forces a condition of thermal equilibrium between the pool and the atmosphere, thus eliminating the necessity to calculate the pool-to-atmosphere heat and mass exchange. This modeling has the adverse effect of over-predicting the heat losses from the cell and allowing credit to be taken for heat sinks that are not, in fact, fully available until the pool temperature is sufficiently high to facilitate sodium vaporization from the pool surface and subsequent condensation on structures above the pool. The condensation and vaporization models are equally crude, so that

subsequent to the energy transfer calculation, if the reactor cavity pool temperature is above the saturation temperature corresponding to the cavity cell pressure, the amount of sodium which will reduce the pool temperature to saturation is non-mechanistically transferred from the pool to the cavity atmosphere. Conversely, if the partial pressure of sodium vapor is above the saturation pressure, the excess sodium vapor is non-mechanistically condensed and "rained" back into the pool.

It is the purpose of this report to describe and present the analytical development and evolution of the CONAN code, as well as presenting the results of comparisons between the CACECO and CONAN codes. In addition, the CONAN code has been used to study the effects of phenomena such as condensation and vaporization which are not mechanistically treated in the CACECO code.

II. AN ADIABATIC ENERGY-MASS BALANCE MODEL

As a check in evaluating both the CACECO and the CONAN energy models, a very simple adiabatic flow model was devised. The model yields a closed-form solution which can be used to compare directly with the more complex codes in the appropriately limited cases.

The physical situation consists of two adiabatic cells which are connected by a flow path (see Figure 1). Cell Number 1 has a pressure different from Cell Number 2, while the cell temperatures may be the same or different. At the outset of the calculation (time = 0), a hypothetical valve between the two cells is opened and an adiabatic expansion of the high pressure cell into the low pressure cell occurs.

Starting with the basic energy equation for an open system:

$$\dot{Q} + \dot{m}_e \left(h_e + \frac{\dot{x}_e^2}{2} + gZ_1\right) - \dot{m}_\ell \left(h_\ell + \frac{\dot{x}_\ell^2}{2} + gZ_2\right) = \frac{d(mu)}{dt} \qquad (1)$$

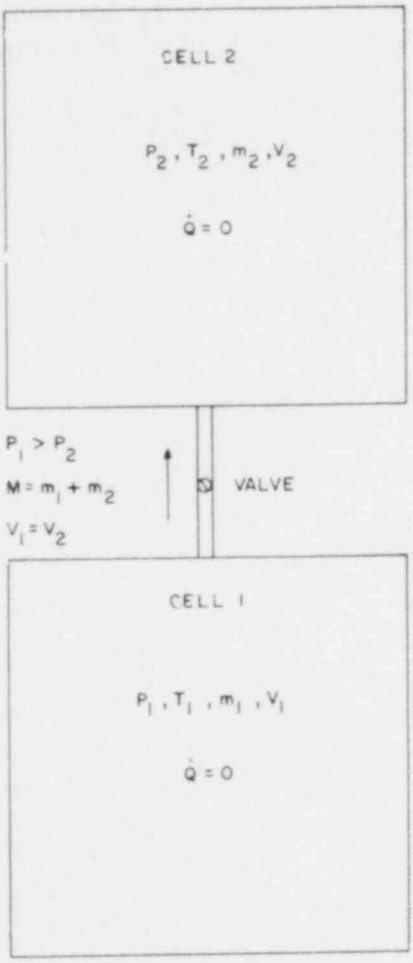

Figure 1. Adiabatic Two Cell Model

If we assume that the kinetic energy and the gravitational potential energy are negligible compared with the internal energy, Eq. (1) reduces to:

$$\dot{Q} + \dot{m}_e h_e - \dot{m}_\ell h_\ell = \frac{d\,(mu)}{dt} , \tag{2}$$

where Q is the rate of energy input into the system, m_e and h_e are the flowrate and enthalpy of the gas entering the control volume, $\dot{m}_\ell$ and h_ℓ are the corresponding flowrate and enthalpy of the gas leaving the volume, and u is the internal energy. Eq. (2) simply says that the rate of energy entering, minus the rate of energy leaving, equals the rate of energy being stored in the system.

In the present system only one flow path exists between the two cells, so that material is either entering or leaving, but not both at once. Thus, imposing this restriction together with the adiabatic condition ($\dot{Q} = 0$), we can further simplify as follows:

$$\dot{m}h = \frac{d\,(mu)}{dt} . \tag{3}$$

Substituting for the internal energy and enthalpy there derives,

$$\frac{d}{dt}\,(mC_vT) = C_pT\dot{m}, \text{ or}$$

$$C_vT\,\frac{dm}{dt} + C_vm\,\frac{dT}{dt} = C_pT\,\frac{dm}{dt}$$

and multiplying by dt yields the final form of the equation,

$$C_vTdm + C_vmdT = C_pTdm \tag{4}$$

If the high pressure cell is indicated as Cell 1, Eq. (4) can be integrated immediately for this cell, with the result,

$$T_1 = T_{10}\left(\frac{m_1}{m_{10}}\right)^{\gamma-1} , \tag{5}$$

where T_{10} and m_{10} are the initial temperature and gas mass in Cell 1. Assuming ideal gases, so that,

$$P_1 = \frac{m_1 R T_1}{V_1} , \tag{6}$$

and substituting Eq. (6) into Eq. (5), the pressure in Cell 1 is derived,

$$P_1 = P_{10} \left(\frac{m_1}{m_{10}} \right)^{\gamma} . \tag{7}$$

In the low pressure cell (Cell 2), which is receiving mass from Cell 1,

$$C_v T_2 dm_2 + m_2 C_v dT_2 = -C_p T_1 dm_1 ,$$

but $dm_1 = -dm_2$ so that, when we include the expression for T_1, we get,

$$\frac{dT_2}{dm_2} + \frac{T_2}{m_2} = \frac{\gamma T_{10}}{m_2} \left(\frac{M - m_2}{m_{10}} \right)^{\gamma-1} . \tag{8}$$

In Eq. (8), M is the total gas inventory (in both cells) and is constant ($m_1 + m_2 = M$). The differential equation in (8) can be solved by first obtaining a solution to the homogeneous equation,

$$\frac{dT_2}{dm_2} + \frac{T_2}{m_2} = 0,$$

which yields

$$T_{2_h} = \frac{C}{m_2} .$$

Eq. (8) can then be integrated using the variation of parameters method, which consists of assuming that the constant of integration is a function of the independent variable m_2,

$$C = f(m_2).$$

When this is done the expression for the low pressure cell temperature is derived:

$$T_2 = \frac{m_{20}}{m_2} T_{20} + \frac{m_{10}}{m_2} T_{10} \left[1 - \left(\frac{m_1}{m_{10}} \right)^{\gamma} \right] \tag{9}$$

Again, assuming an ideal gas, the pressure in Cell 2 is found to be,

$$P_2 = P_{20} + \left(\frac{V_1}{V_2} \right) P_{10} \left[1 - \left(\frac{m_1}{m_{10}} \right)^{\gamma} \right] \tag{10}$$

Finally, we can obtain the equilibrium pressure by setting Eqs. (7) and (10) equal and solving for the ratio m_1/m_{10}. When this is done we obtain the result that, regardless of the initial temperatures in the two cells, and for an ideal gas

$$P_{equil} = \frac{V_1 P_{10} + V_2 P_{20}}{V_1 + V_2} \quad . \tag{11}$$

III. COMPARISON OF ADIABATIC MODEL BETWEEN CACECO and CONAN

A series of cases were run with the CACECO code in which all of the heat structures were removed, together with the chemical reactions. The various modeling options available were supressed in order to model the very simple situation described above. Pure nitrogen gas at varying temperatures and pressures was used. The code was run until the cells came into mechanical equilibrium.

Figures 2 and 3 show the results for a typical comparison case (Case 1 in this report). In the case shown, the initial temperature in both cells was 293°K (528°R), while the Cell 1 initial pressure was 10 atms and the Cell 2 initial pressure was 1 atm. The cell volumes were made equal. Figure 2 shows the pressure in both cells as a function of the quantity of gas transferred (or more accurately, the ratio of mass to initial mass in the donor cell). Although the CACECO code calculated an equilibrium pressure that agrees with the present model, it predicted a considerably larger mass transfer. The present analysis indicates that 35% of the Cell 1 gas should be transferred into Cell 2, whereas CACECO predicts that 43.5% will be transferred. Inspection of Figure 3 will show why this occurs. This figure shows the cell temperatures as a function of m_1/m_{10}. This analysis predicts a significantly larger energy transfer than that calculated by the CACECO code. Due to the higher heat transfer rate calculated using the present model, the back pressure in Cell 2 develops more

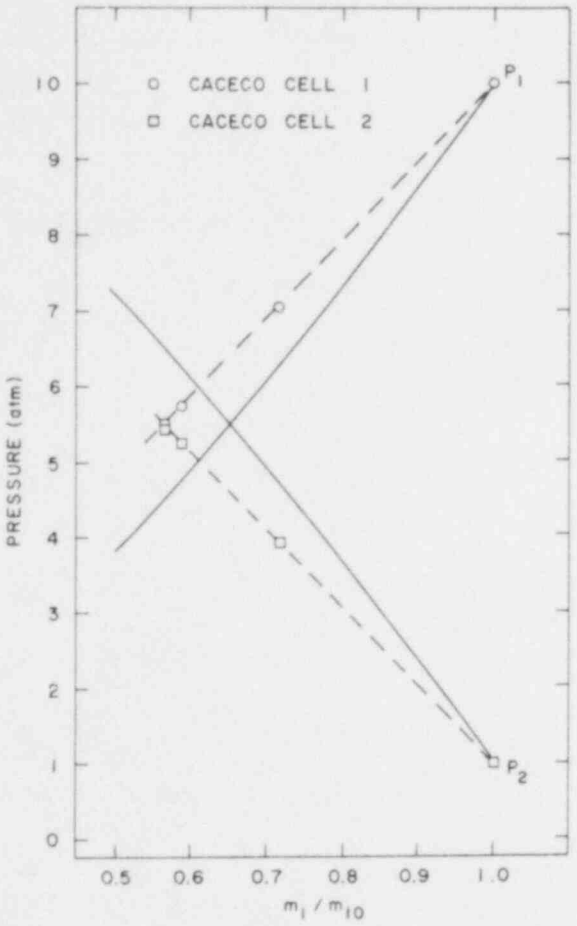

Figure 2. Comparison of CACECO Pressures with Exact Solution for Adiabatic System

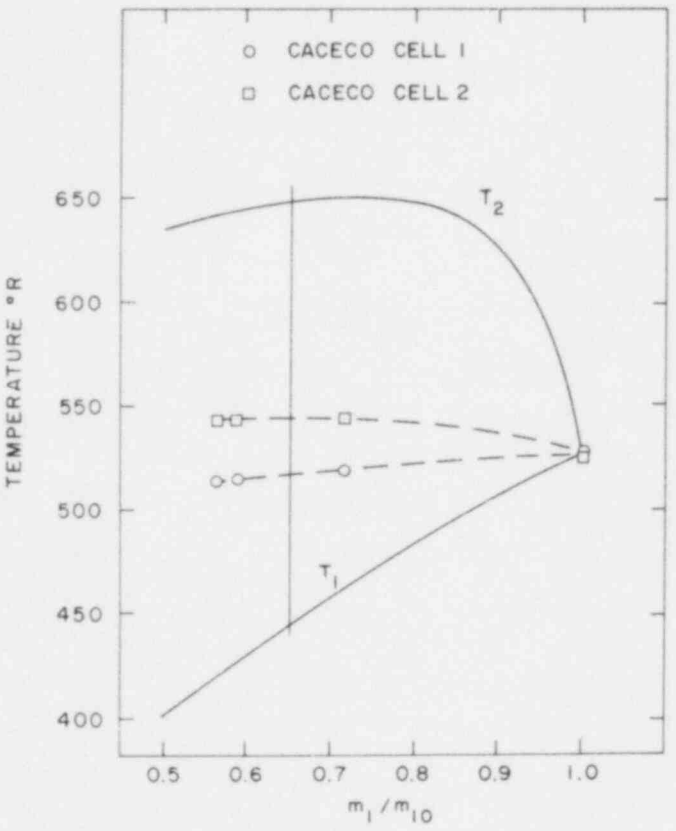

Figure 3. Comparison of CACECO Temperatures with Exact Solution for Adiabatic System

rapidly and equilibrium pressure is obtained with a smaller quantity of total displaced gas.

Due to the simplicity of the model described here and to the fact that it does not depend on temperature-dependent heat capacities, it is believed to be a reasonably good debugging check case for the CACECO code. The energy modeling problem has been called to the attention of the CACECO authors who have subsequently identified and eliminated the error.

An identical case was calculated using the CONAN code in order to verify its accuracy with regard to the same parameters. Similarly, the results were compared to the adiabatic model and these are shown in Figures 4 and 5. These figures indicate quite good agreement with both primary and secondary temperatures and pressures.

IV. FORMULATION AND DESCRIPTION OF THE CONAN CODE MODELING

The CONAN code employs a numerical integration package to solve the system of 15 first-order differential equations which arise from the continuity, energy, and momentum equations for a two-cell system. The code, as it presently stands, includes only one chemical reaction, namely, the combustion of sodium vapor,

$$4\ Na(V) + O_2 \rightarrow 2\ Na_2O + h_{react}.$$

It does not allow for the presence of water vapor and its associated chemical reactions in the system The code does not include sodium-concrete reactions, and therefore is limited to cases in which the cell liners remain intact. These two parameters, water vapor production and the sodium-concrete reaction, could be incorporated into the CONAN code; the latter with comparative ease, and the former with some difficulty.

The CONAN code, unlike the CACECO code, incorporates two separate types of heat structures. These are termed here as (1) heat structures, and (2) heat

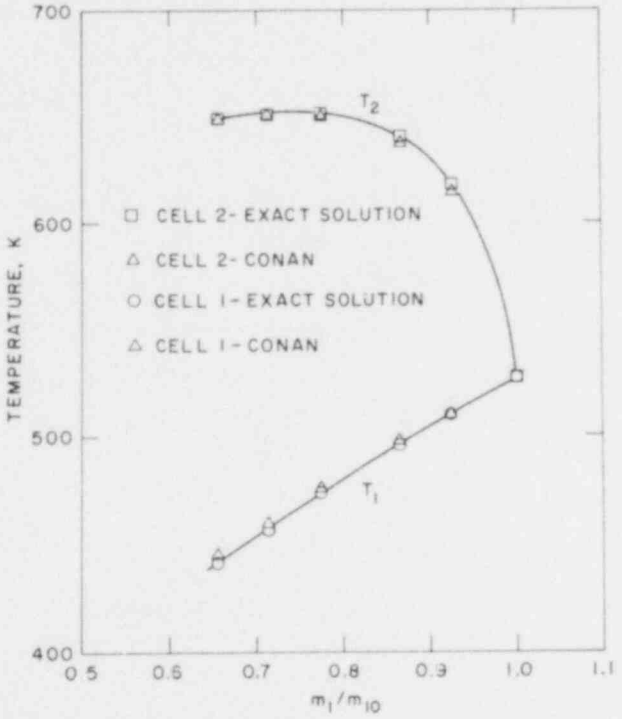

Figure 4. Comparison of CONAN Temperatures with Exact Solution for Adiabatic System

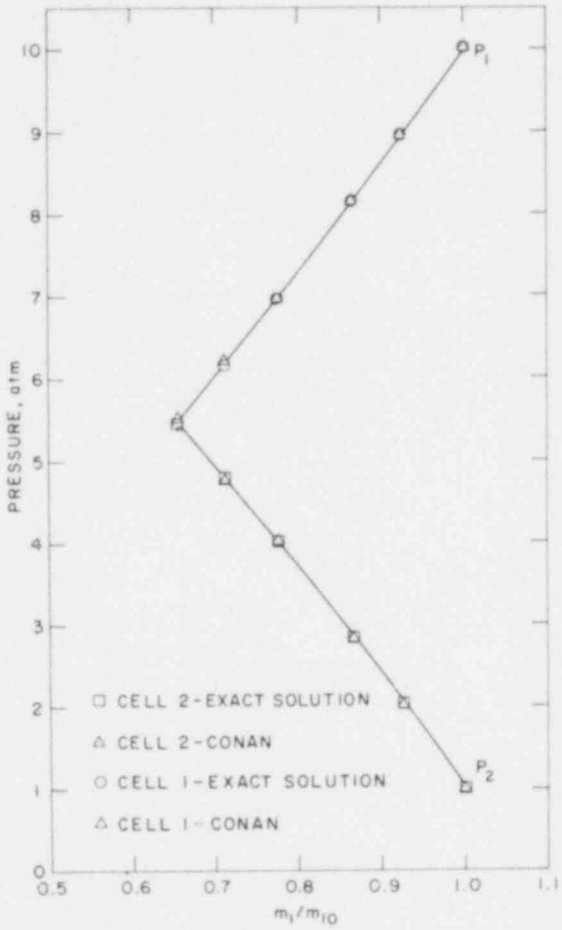

Figure 5. Comparison of CONAN Pressures with Exact Solution for Adiabatic System

sinks. These are differentiated by the method of solution. For the heat structures, the one-dimensional transient heat conduction equation is employed, together with an explicit numerical method to calculate the temperature profile. Heat structures are used to model materials which have relatively low thermal conductivity, i.e., concrete, firebrick, and vessel insulation. Heat sinks are handled as lumped parameters and the temperature is assumed to be constant throughout the region. The temperature is found by integrating the net heat flux into and out of the heat sink,

$$\int_{t_1}^{t_2}\left[\dot{Q}_{in}(t) - \dot{Q}_{out}(t)\right] dt = M_{sink}\int_{T_1}^{T_2} C_p(T)dT \qquad (12)$$

Heat sinks are used to model materials which have relatively high thermal conductivities such as steels and other metallic materials.

Heat transfer between atmospheres and surfaces is calculated using radiation and Nusselt number correlations for natural convection heat transfer. The first version of the CONAN code did not incorporate the phenomena of condensation or vaporization either in their heat transfer effects or their recirculation effects. The CACECO code can incorporate the heat transfer effects due to condensation since the heat transfer coefficients are not calculated internally, but rather are input in table form as function of time or temperature. This procedure is, however, inadequate due to the neglected, but nevertheless significant, effect of non-condensible gases on the condensation rate. Failing to incorporate condensation heat transfer on surfaces inside the reactor cavity, however, may not have significant effects on the calculation of heat losses out of the cavity (into the surrounding concrete structures). Although condensation heat transfer coefficients are significantly higher than those due to natural convection and radiation at the temperatures involved, heat transfer out of the cavity is limited by the gap resistance between liner and concrete, and by radiation.

Starting with the basic energy equation for each volume, we have,

$$\frac{\partial}{\partial t}(um) + \dot{m}_{\ell} h_{\ell} - m_e h_e = \dot{Q}. \tag{13}$$

The $\dot{Q}$ term in general contains the decay heat, chemical reaction energy, and heat losses,

$$\dot{Q} = h_{comb} R_{comb} + \dot{Q}_D - \sum_i h_i A_{w_i} (T - T_{w_i}) \tag{14}$$

where h_{comb} is the heat of combustion, R_{comb} is the reaction rate, and $\dot{Q}_D$ is the decay heat directed into that volume. The last term is, of course, the sum of the heat loss terms. If the subscripts p, 1 and 2 refer, respectively, to the pool (which is located in Cell 1), the Cell 1 atmosphere, and the Cell 2 atmosphere, and the flow is from Cell 1 to Cell 2 ($p_1 > p_2$), then we can write the energy equations as follows:

For the Sodium Pool

$$Q_D - h_{pw} A_{pw} (T_p - T_{pw}) - h_{p1} A_{p1} (T_p - T_1) - (\dot{m}_{s1} + \dot{m}_{s12}) h_{svp} = - (\dot{m}_{s1} + \dot{m}_{s12}) u_{s1p} + m_p \dot{u}_{s1p}. \tag{15a}$$

For the Cell 1 Atmosphere

$$h_{p1} A_{p1} (T_p - T_1) - h_{w1} A_{w1} (T_1 - T_{w1}) + (\dot{m}_{s1} + \dot{m}_{s12}) h_{svp} - \dot{m}_{N12} h_{N1} - \dot{m}_{s12} h_{sv1} = \dot{m}_{s1} u_{sv1} - \dot{m}_{N12} u_{N1} + m_{s1} \dot{u}_{sv1} + m_{N1} \dot{u}_{N1} + m_{NO1} \dot{u}_{NO1}, \tag{15b}$$

For the Cell 2 Atmosphere

$$h_{comb} \dot{m}_{s12} - h_{w2} A_{w2} (T_2 - T_{w2}) + \dot{m}_{N12} h_{N1} + \dot{m}_{s12} h_{sv1} - \dot{m}_{O23} h_{O2} - \dot{m}_{N23} h_{N2} = - (\dot{m}_{O23} + \dot{m}_{Ocomb}) u_{O2} + (\dot{m}_{N12} - \dot{m}_{N23}) u_{N2} + \dot{m}_{NO2} u_{NO2} + m_{N2} \dot{u}_{N2} + m_{O2} \dot{u}_{O2} + m_{NO2} \dot{u}_{NO2}. \tag{15c}$$

If the pressure is higher in Cell 2 ($P_2 > P_1$), the equations become:

For the Sodium Pool

$$Q_D - h_{pw}A_{pw}(T_p - T_{wp}) - h_{pl}A_{pl}(T_p - T_l) - (\dot{m}_{sl} + \dot{m}_{scomb})h_{svp} =$$
$$- (\dot{m}_{sl} + \dot{m}_{scomb})u_{slp} + m_p \dot{u}_{slp}, \qquad (16a)$$

For the Cell 1 Atmosphere

$$h_{comb}\,\dot{m}_{scomb} + h_{pl}A_{pl}(T_p - T_l) - h_{wl}A_{wl}(T_l - T_{wl})$$
$$+ \dot{m}_{N21}\,h_{N2} + \dot{m}_{O21}\,h_{O2} + (\dot{m}_{sl} + \dot{m}_{scomb})h_{svp} = \dot{m}_{N21}\,u_{Nl}$$
$$+ \dot{m}_{sl}\,u_{Nl} + \dot{m}_{sl}\,u_{svl} + \dot{m}_{NOl}\,u_{NOl} + m_{sl}\,\dot{u}_{svl} + m_{Nl}\,\dot{u}_{Nl}$$
$$+ m_{NOl}\,u_{NOl} \qquad (16b)$$

For the Cell 2 Atmosphere

$$- h_{w2}A_{w2}(T_2 - T_{w2}) - (\dot{m}_{O23} + \dot{m}_{O21})h_{O2} - (\dot{m}_{N23} + \dot{m}_{N21})h_{N2} = - (\dot{m}_{O23} + \dot{m}_{O21})u_{O2}$$
$$- (\dot{m}_{N21} + \dot{m}_{N23})\,u_{N2} + m_{N2}\,\dot{u}_{N2} + m_{O2}\,\dot{u}_{O2} + m_{NO2}\,\dot{u}_{NO2}. \qquad (16c)$$

The above set of equations do not include all the heat transfer terms. For example, radiation from the pool surface to the cavity walls and reactor vessel or from the Cell 2 atmosphere to the equipment in that cell is ignored. These terms were avoided in order to make the equations more tractable. (For definition of terms, see the nomenclature on page 55.) The essential difference in the two sets of equations lies in the fact that sodium combustion is occurring in Cell 2 in the first case, while it occurs in Cell 1 in the second case.

Because the dynamics of condensation and pool boiling were neglected in Version 1 of the code, some assumptions and simplifications had to be made regarding the sodium vaporization rate and the atmospheric partial pressure of sodium in Cell 1. Apart from core-disruptive energetics and chemical explosions, containment transients in the LMFBR can be relatively long term events with physical processes occurring rather slowly for the most part. For this reason the dynamics of pool boiling were neglected in this version, and the assumption was made that the partial pressure of sodium vapor in the Cell 1

atmosphere was equal to the saturation pressure of sodium vapor at the pool temperature. The saturation pressure is calculated from correlations given in Golden and TOKAR[2] of the type:

$$P_{s1} = P_{sat} = T_p^{C_s} e^{A_s + B_s/T_p}. \tag{17}$$

The mass of sodium vapor in the Cell 1 atmosphere, m_{s1}, is then calculated using a slightly augmented equation of state which accounts for the non-ideal characteristic of sodium vapor,

$$m_{s1} = \frac{V_1 T_p^{C_s} e^{A_s + B_s/T_p}}{T_1 (A_R T_1^2 + B_R T_1 + C_R)} \tag{18}$$

where V_1 is the Cell 1 volume, and the quadratic function in the numerator is a curve fit of the gas constant for sodium vapor. The rate of change of the sodium vapor mass in the Cell 1 atmosphere is then the time derivative of Eq. (15), namely,

$$\dot{m}_{s1} = \frac{V_1 P_{s1} \left[\frac{C_s}{T_p} - \frac{B_s}{T_p^2}\right] \dot{T}_p}{\left[A_R T_1^3 + B_R T_1^2 + C_R T_1\right]} - \frac{V_1 P_{s1} \left[3A_R T_1^2 + 2B_R T_1 + C_R\right] \dot{T}_1}{\left[A_R T_1^3 + B_R T_1^2 + C_R T_1\right]^2} \tag{19}$$

The sodium boiloff rate must be equal to the rate of increase of sodium vapor in the atmosphere, which is due to the change in saturation condition, plus the rate of removal of sodium vapor from the atmosphere in the one case due to venting into Cell 2, and in the other case due to combustion in Cell 1. Thus, in Eq. (15a), the rate of evaporation from the pool is $(\dot{m}_{si} + \dot{m}_{s12})$ where $\dot{m}_{s12}$ is the mass transport rate (by venting) of sodium vapor from Cell 1 to Cell 2. Likewise, the corresponding term in Eq. (16a) is $(\dot{m}_{s1} + \dot{m}_{scomb})$ where $\dot{m}_{scomb}$ is the rate of sodium combustion as oxygen is introducted into Cell 1 from Cell 2.

The sodium combustion process is not modeled using chemical kinetics, but is assumed to go to completion instantaneously as sodium vapor and oxygen come into contact. The sodium combustion rate is therefore calculated in Cell 2 as the flow rate of sodium vapor, $\dot{m}_{s2}$ or:

Reaction Rate = $\dot{m}_{s12}$ (kg/sec).

If flow is in the reverse direction,

Reaction Rate = $\dot{m}_{scomb} = 2.875\ \dot{m}_{021}$,

where 2.875 is the stoichometric ratio for the reaction and $\dot{m}_{021}$ is the mass transport rate of oxygen from Cell 2 to Cell 1.

The cell-to-cell mass transport rate is calculated using a simple nozzle equation,

$$\dot{m}_{12} = C_{12}A_{12}\sqrt{\rho_1(P_1 - P_2)} \tag{20}$$

The CACECO code uses the same type of nozzle equation to calculate flow rates, but in addition employs what are termed "leakage flow rates". Both models are ΔP-driven flows and are, in fact, interchangeable. In Eq. (20), C_{12} is the nozzle coefficient, A_{12} is the cross sectional area of the flow path, and ρ_1 is the gas density. A similar equation is used to describe the leakage path from the containment building (Cell 2) to the outside atmosphere. These terms appear in Eqs. (15c) and (16c) as $\dot{m}_{N23}$ and $\dot{m}_{023}$, and refer to the nitrogen and oxygen leak rates, respectively.

Pressures are calculated by summing the partial pressures of the constituents and employing the ideal gas flow in the following manner:

$$P_1 = P_{s1} + P_{N1}, \tag{21}$$

$$P_2 = P_{02} + P_{N2}, \tag{22}$$

where

$$P_{N1} = m_{N1}R_N T_1/V_1, \tag{23}$$

$$P_{N2} = m_{N2}R_N T_2/V_2, \tag{24}$$

$$P_{02} = m_{02}R_0 T_2/V_2. \tag{25}$$

When the appropriate internal energy functions are input to the various equations (15a-c and 16a-c), the differential equations for the temperatures $\dot{T}_1$, $\dot{T}_2$ and $\dot{T}_p$ can be expressed in terms of the other system variables.

In addition, the mass balance equations are expressed in differential form and the resulting set of coupled equations are solved in a step-wise manner, using an existing integration package.

The CONAN code incorporates a subroutine which uses an explicit finite difference method to solve the one-dimensional transient heat conduction equation in the heat structures. The heat structures model such things as concrete, firebrick, and insulation.

V. RESULTS AND COMPARISONS

The version of CONAN described in Section IV, although not yet containing models for evaporation and condensation, was sufficiently complete to allow for comparisons between CACECO and CONAN with regard to non-adiabatic cases and configurations in which a sodium pool is present.

The first case of interest, therefore, was one in which the effect of sodium heatup, boiloff and combustion could be isolated and studied separately from other effects. With this in mind, a test case (Case 2) was devised in which the sodium-containing cell was assumed to be adiabatic and the decay heat (for FFTF) was used entirely to heat up and vaporize the sodium. In order to accomplish this, heat sinks and structures were completely eliminated in the reactor cavity (sodium containing cell). The reactor containment building was modeled, however, with two heat sinks, which consisted of the reactor building steel shell and the equipment contained therein. This was necessary since the quantity of energy released during the combustion of sodium vapor in the RCB would have driven the temperature over 8000°K, if heat losses in the RCB had not been considered.

The two cells in Case 2 were modeled with the dimensions and volumes approximating those of the Fast Flux Test Facility (FFTF), as is the case for all

the cases discussed in this report. In addition, the FFTF sodium inventory of 281,226 kg was also used.

Both of the codes were furnished with identical heat transfer coefficients between the atmosphere and the two heat structures in the RCB. Care was taken to assure that the thermophysical properties which are not hard-coded (those for heat structure materials) were comparable. However, because the CACECO code reads and interpolates thermophysical properties from input tables, while CONAN uses functional curve fits, the values employed by the codes are obviously not exactly identical. This is also true of the decay heat curve which was curve-fit using data points from the FFTF Thermal Margins Report.(3)

Figure 6 shows the pertinent CONAN generated temperature transients for Case 2. The case was started with an initial pool temperature of 820°K and an initial ambient temperature of 300°K. The sodium boiling temperature is attained at about 9.2 hours and the cavity atmospheric temperature reaches the pool temperature about 2 hours after incipient boiling. The RCB atmospheric and heat structure temperatures appear to be in reasonable relationship, the atmosphere being hotter, and the heat structures which receive heat from the atmosphere somewhat cooler. The RCB equipment temperature is higher than the shell temperature, since the shell is losing heat to the outside air by convection.

The comparisons between CACECO and CONAN for Case 2 are shown in Figures 7 through 13. The sodium pool temperature is given in Figure 7. Although the overall agreement between the two codes is reasonably good for Case 2, the primary difference appears to occur during the pre-boiling period. This is seen clearly in the pool temperature, which indicates a slightly higher level for the CONAN results prior to boiling. This is due to the basic difference in the boiling models between the two codes. For Case 2 the CACECO code was provided

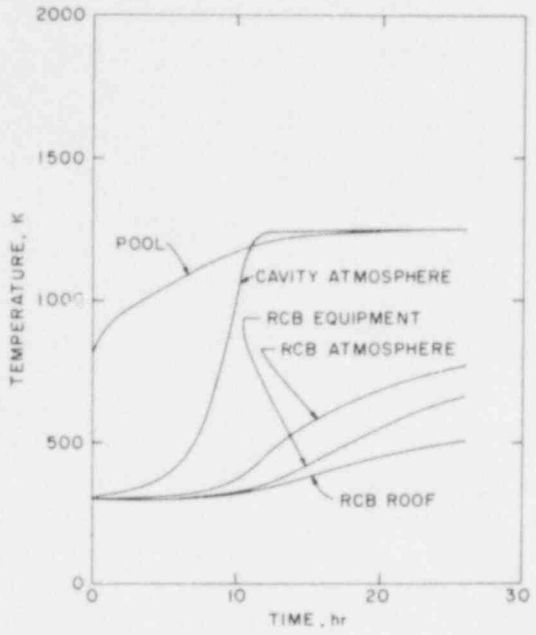

Figure 6. CONAN Temperatures for Case 2

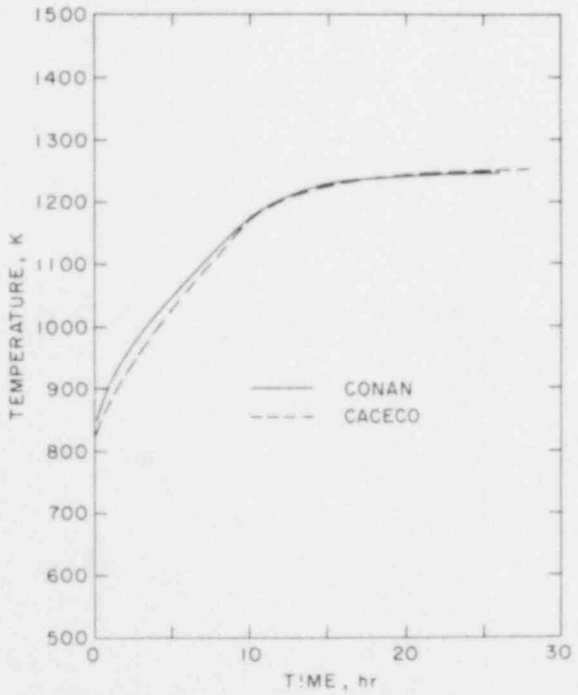

Figure 7. Comparison of Sodium Pool Temperatures for Case 2

with a special update which over-rides the Cell 1 temperature equilibrium condition by incorporating a subroutine called POOLR. This subroutine, among other things, calculates heat transfer from the pool to the atmosphere as well as evaporative mass transfer between the pool surface and the atmosphere. Since the heat transfer coefficients in Cell 1 of the CONAN code were all set to zero for this case, it was also necessary to set the corresponding heat transfer coefficients in POOLR to zero. Due to the evaporation model used in POOLR, which uses a heat transfer simulation model, the evaporation rate was in effect also set equal to zero. Thus, prior to boiling no mechanism was available in CACECO to transfer sodium from the pool to the atmosphere. The CONAN code, in the present version, forces the atmosphere partial sodium pressure to the saturation pressure of sodium corresponding to the pool temperature. The total Cell 1 pressure is higher for the CONAN code, and this is reflected in the pool heating rate.

The Cell 1 (reactor cavity) atmospheric temperature is presented in Figure 8. The pre-boiling modeling differences are seen clearly in this figure. The lack of pool-to-surface heat and mass transfer in the CACECO pre-boiling phase results in a nearly constant gas temperature, followed during the boiling phase by a sharp rise in the temperature and attainment of reasonably good agreement with the boiling phase as predicted by CONAN.

The Cell 2 (RCB) temperature and pressure are shown in Figures 9 and 10, respectively. As expected from the foregoing, the CACECO code predicted no RCB pressure transient effects until pool boiling had occurred, while CONAN displays very slow pressure and temperature transients which increase as the cavity sodium vapor pressure increases. However, subsequent to boiling, the CACECO predicted containment building pressure and temperature actually exceed those generated by CONAN.

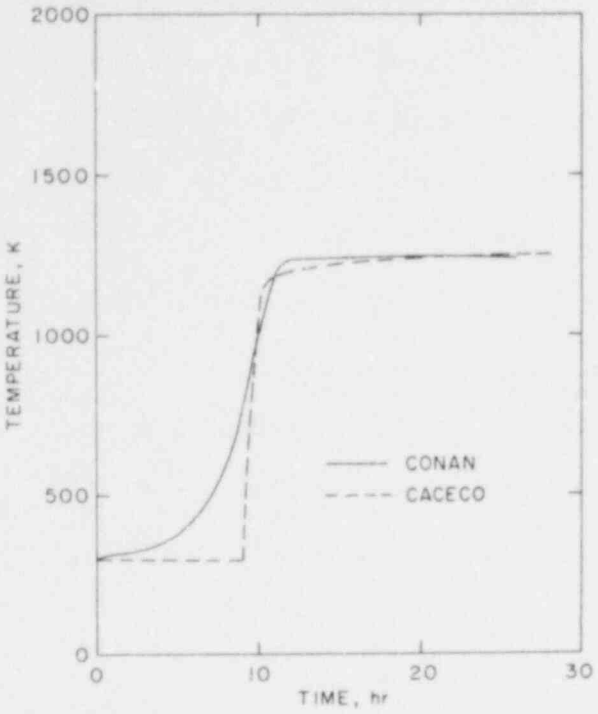

Figure 8. Comparison of Cell 1 Atmospheric Temperature for Case 2

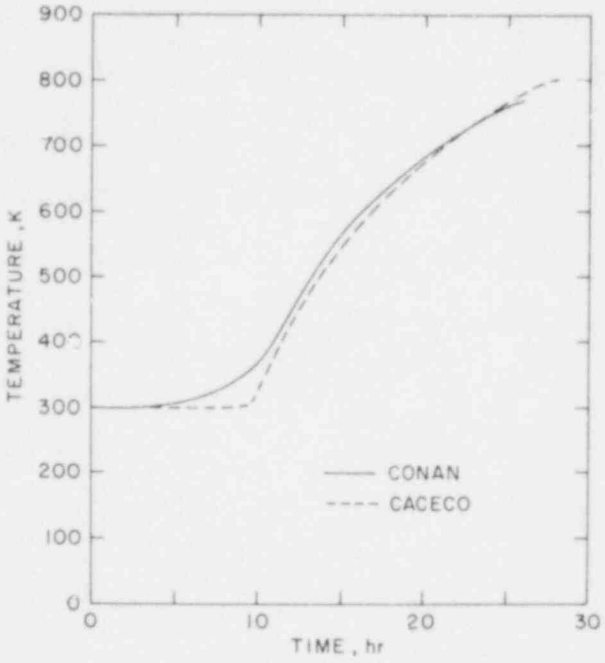

Figure 10. Comparison of Cell 2 Temperature for Case 2

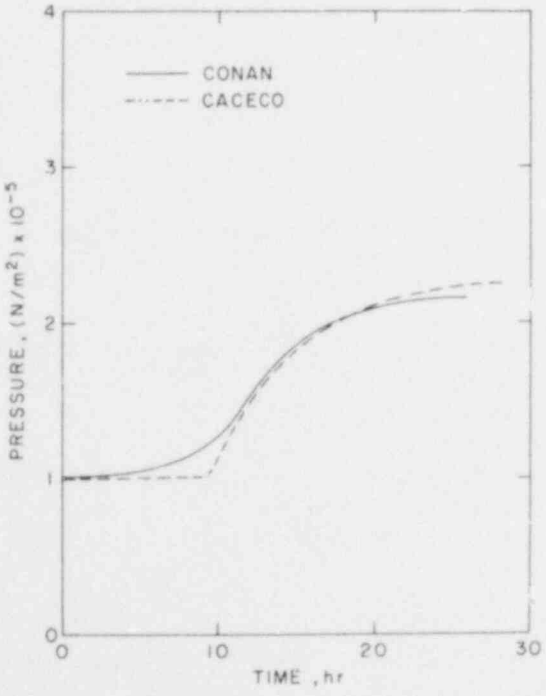

Figure 9. Comparison of Cell 2 Pressure for Case 2

The general characteristics already seen in the atmospheric temperatures are also reflected in the RCB equipment and roof temperatures, Figures 11 and 12. These, of course, tend to verify the heat structure and heat transfer models as utilized in both codes, since the differences seen here are due to the pool boiling models and not the heat transfer models.

The final graph in this sequence gives the RCB oxygen mass as a function of time. Again, the transient is delayed in the CACECO results until pool boiling is attained. However, the curves are very similar, with oxygen depletion occurring at 26.5 and 28.2 hours for CONAN and CACECO, respectively. This indicates that the amount of sodium combustion prior to boiling, as calculated by CONAN, did not have a significant effect on the overall time required to obtain oxygen depletion.

A second case in this sequence (Case 3) was run in order to determine the effect of the additional heat capacity represented by the structures present in the reactor cavity. These structures include the steel in the reactor vessel, reactor head, and cell liners. To simplify the models, only two heat sinks were added to the reactor cavity volume. The first, a mass of 131,600 kgs of steel, was put into contact with the sodium pool, and the second, a mass of 822,000 kgs of steel, was put into contact with the cavity atmosphere. These masses are arbitrary and represent about 1/3 more steel than is actually contained in the vessel and liners. The additional heat capacity was intended to account for some of the heat losses which would occur by conduction through the surrounding concrete. The structures in the reactor containment building were left the same as those in Case 2. Again the heat transfer coefficients between pool and steel and between atmosphere and steel were set equal in CACECO and CONAN.

Figures 14 through 17 show the results for Case 3. The cell atmospheric temperatures, together with the heat structure temperatures, are given in

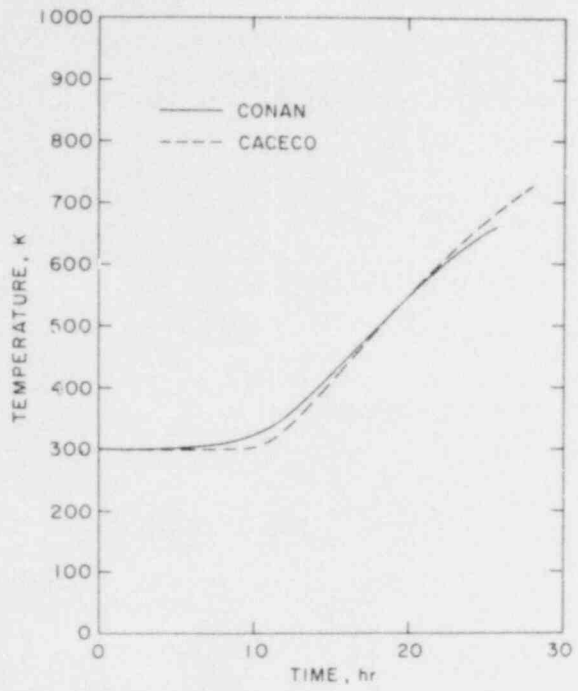

Figure 11. Comparison of Cell 2 Equipment Temperature for Case 2

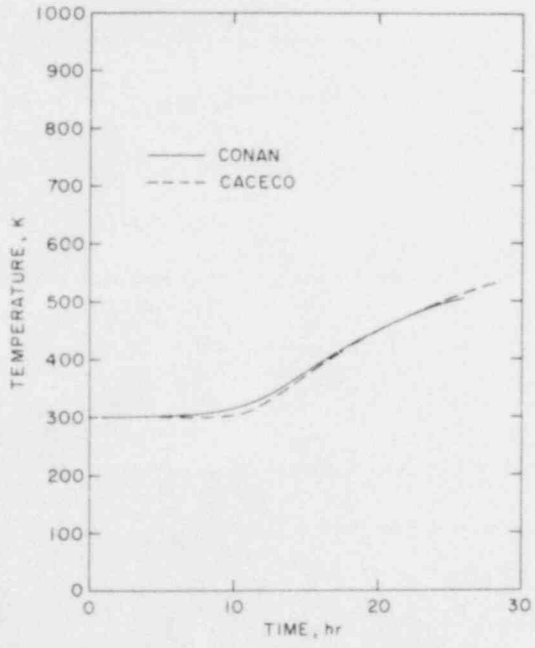

Figure 12. Comparison of Cell 2 Roof Temperature for Case 2

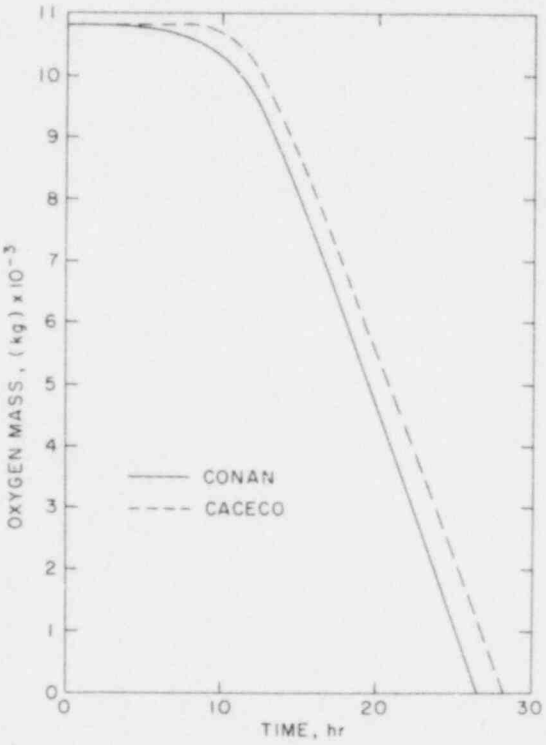

Figure 13. Comparison of Cell 2 Oxygen Inventory for Case 2

Figure 14. Incipient boiling was extended from 9 hours in the adiabatic case to about 24 hours for Case 3. The temperature and pressure responses in the reactor containment building are similarly extended. Of most interest, however, is the reactor cavity atmospheric temperature, which is maintained at a nearly 600°K lower temperature than that of the pool during most of the transient. This is due to the presence of the large mass of ex-pool steel in contact with the cavity atmosphere. Figure 14 shows that the initial steel temperature was assumed to be 300°K but approaches the atmospheric temperature rapidly after pool boiling occurs, being nearly the same (630°K) at the point of oxygen depletion (54 hours). This effect is somewhat exaggerated in Case 3 because the initial steel temperature should probably be nearer to the initial sodium temperature of 820°K. This should be the case, since the accident scenario calls for the sodium and fuel debris to have drained from the reactor vessel at time equal to zero. Previous to that the sodium inventory must have been nearly in thermal equilibrium with the metal of the reactor vessel. In any case, the results show that the atmospheric temperature may be significantly lower than the pool temperature so that condensation on structures above the pool may have a significant effect.

Differences in the temperature responses as calculated by CONAN and CACECO are identified in Figure 15. The Cell 1 temperature transients, including pool, atmosphere, and heat structures, appear to agree reasonably well until incipient boiling occurs. The CACECO code predicted incipient boiling slightly earlier (at about 20 hours), at which time the pool temperature dropped almost immediately down to more than 100°K below the boiling temperature. At the same time the cavity atmospheric temperature began to oscillate rather markedly. Apparently the oscillation is due to the manner in which vaporization from the pool is balanced against sodium condensation and "rainout" from the atmosphere in

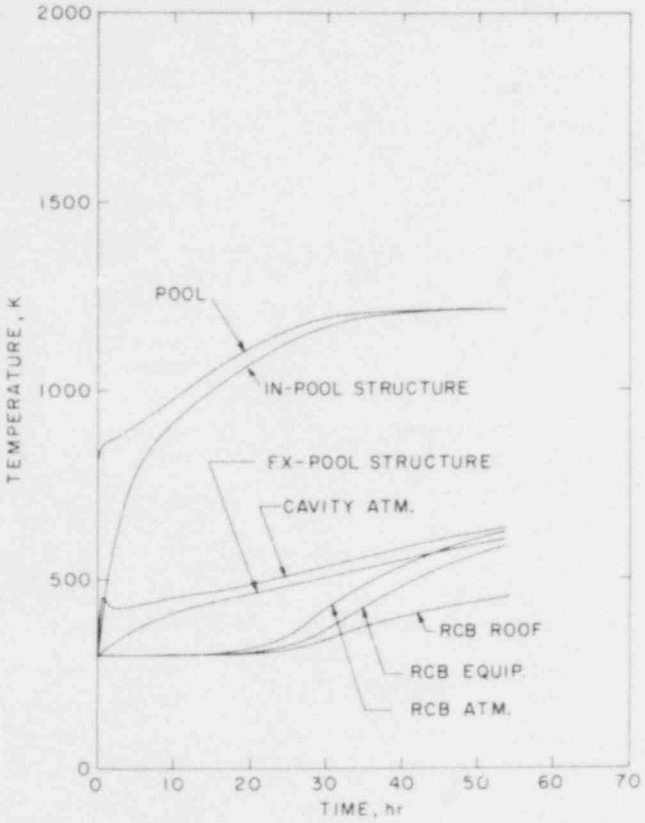

Figure 14. CONAN Temperature Results for Case 3

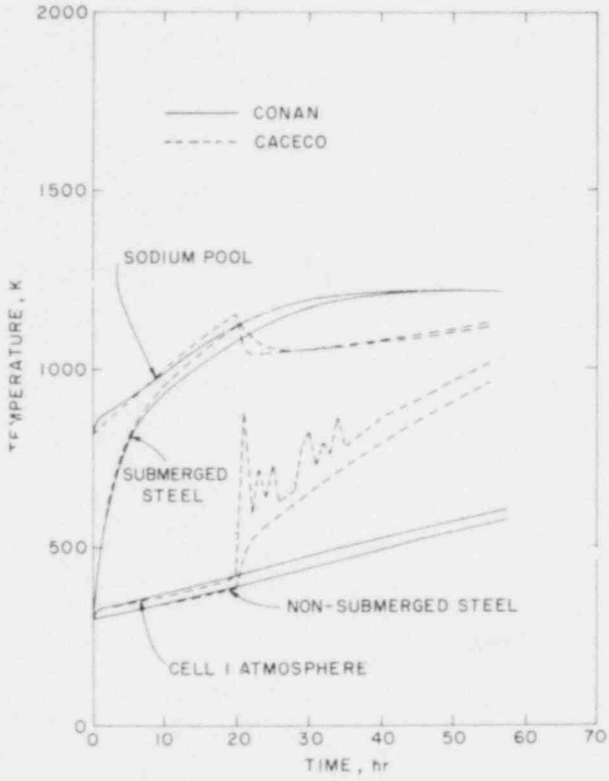

Figure 15. Comparison of Temperature Results for Case 3

CACECO. When the boiling temperature was reached, large quantities of sodium were vaporized. This sodium vapor, when brought into thermal equilibrium with the atmosphere, left the atmosphere super-saturated, resulting in a large non-mechanistic "rainout" of relatively cold liquid sodium back into the pool, thus depressing the pool temperature. This lack of balance between vaporization and condensation (both non-mechanistic) results in an unrealistically high sodium reflux rate.

The CONAN code results do not indicate such a crisis condition at the point of incipient boiling, since in effect this version of the CONAN code does not have a "built in" specific boiling point. Rather the quantity of sodium vapor in the atmosphere is a smooth function of the pool temperature. As discussed earlier, the sodium vapor partial pressure is calculated as the saturation pressure corresponding to the pool temperature. The assumption inherent in this model is that the transient is slow enough such that evaporation is able to keep the atmosphere saturated at all times while condensation does not occur. In terms of containment pressurization these are obviously conservative assumptions; however, it is apparent from these results that condensation may have a significant effect and certainly should be considered.

Figure 16 gives the reactor cavity and RCB pressures for this case. The obvious anomaly here is the fact that in the CACECO case a vacuum condition occurs in the reactor cavity subsequent to boiling. This is again due to a combination of CACECO modeling problems. The standard version of CACECO does not allow reverse flow for situations in which the pressure gradient is reversed (in this case, when the RCB pressure exceeds the cavity pressure). Therefore, during the initial boiling-driven transient, the sudden addition of heat and sodium vapor into the cavity atmosphere drove the pressure up, resulting in quantities of nitrogen and sodium vapor being vented into the RCB. During the subsequent

condensation phase gases were not allowed to flow from the RCB back into the cavity to equalize the pressures, and thus the cavity pressure was actually reduced to less than 0.4 atm. Apart from the pressure generated by the sodium vapor, which was vented and burned immediately after incipent boiling, the RCB pressures predicted by CACECO are quite benign. This is, of course, due to the drop in pool temperature after boiling. The reason is easily seen in Figure 17, which shows the RCB oxygen mass. The cavity vacuum prevents venting of sodium vapor into the RCB, or oxygen into the cavity, thus preventing combustion and pressurization.

The foregoing cases have demonstrated that CACECO and CONAN do not agree subsequent to the onset of boiling. Although the CACECO boiling and condensation models are somewhat crude, they demonstrate that the effect of the onset of boiling probably has a more dramatic effect than that predicted by the CONAN version which has been utilized thus far. It was deemed necessary, therefore, to incorporate evaporation and condensation models into the CONAN code. It is also apparent from Case 3 that these models should be more mechanistic than those in the CACECO code. The next section discusses the development of condensation and vaporization models.

VI. CONDENSATION AND EVAPORATION MODELS

The problem of the condensation of sodium vapor on the surfaces and structures above the pool in the reactor cavity is complicated by the presence of large quantities of non-condensable gases. The condensation rate cannot, therefore, be treated as in the classical Nusselt condensation problem. Condensation of vapors in the presence of non-condensables has been widely investigated[4,5,6] for steam condensation on cooled surfaces. In general, the solutions are rather complicated and require iterative methods. Fortunately,

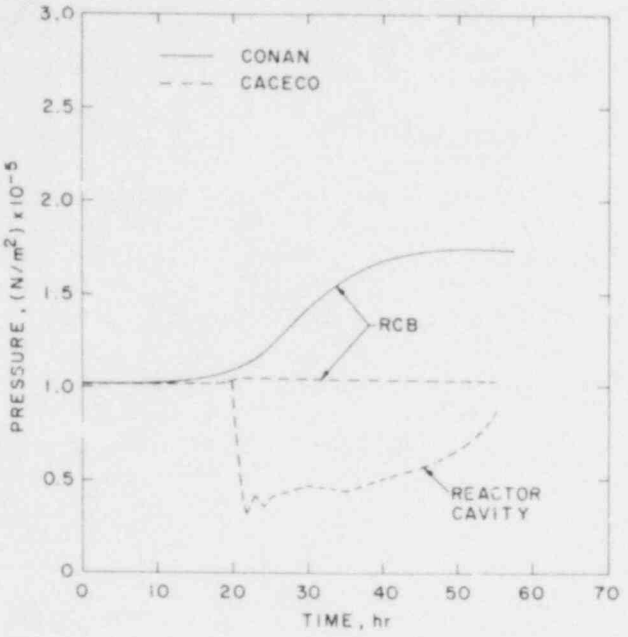

Figure 16. Comparison of Pressures for Case 3

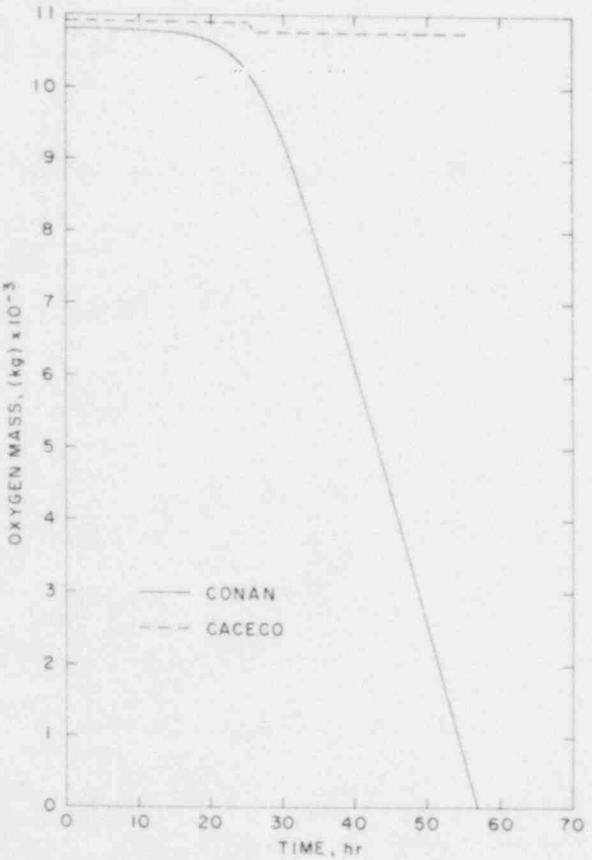

Figure 17. Comparison of Cell 2 Oxygen Inventory Core Case 3

however, for the film-wise condensation of sodium on vertical surfaces, the solution does not require iteration and is fairly straightforward.

The complicated geometry associated with the structures present in the cavity make an exact solution for all the structural configurations unwieldy. For this reason, and since more accurate solutions are not justified when weighed against the many uncertainties involved, a rather approximate method of solution was chosen for both the condensation and evaporation phenomena. The method used here incorporates a similarity solution which entails calculating the heat transfer rate and then employing a parameter which describes the relationship between diffusion and heat transfer to determine the sodium vapor diffusion rate.

In the absence of non-condensable gases, the liquid sodium film thickness at the wall is calculated as a function of vertical position on the wall,

$$\delta = \left(\frac{4z\mu k(T_s - T_w)}{\rho_\ell(\rho_\ell - \rho_v)gh_{fg}} \right)^{1/4} \tag{26}$$

Equating the conductive heat flux through the film with an effective heat transfer coefficient yields the classical Nusselt expression for the heat transfer coefficient, which, when averaged over the vertical extent of the wall, yields,

$$h = 0.943 \left(\frac{g\rho(\rho-\rho_v)k^3 h_{fg}}{(L\mu(T_s-T_w)} \right)^{1/4} \tag{27}$$

In the absence of non-condensable gases, the vapor-liquid interface is at the same temperature, T_s, as that of the bulk vapor, namely, the temperature which corresponds to the vapor saturation pressure. However, with even very minute quantities of non-condensables present, significant concentrations of non-condensables will accumulate at the film-gas interface. The effect of these non-condensables is that, in order to arrive at the film surface and condense

there, the sodium vapor must diffuse through the gases near the interface. The non-condensables accumulate near the interface since they are carried there in the same manner as the vapor, but unlike the vapor they are not removed by condensation and can, therefore, only be removed by diffusing back through the surrounding vapor. The result is that a gas concentration gradient is established with the highest concentration being located at the film interface. Thus, the sodium vapor pressure at the interface is lower than it is in the bulk vapor, and the interface temperature is the saturation temperature which corresponds to the partial pressure of sodium vapor at the interface. The difficulty arises because the interface temperature is not known explicitly, and, therefore, must be determined in the solution. This is usually accomplished by iterating on the interface temperature.

The similarity solution employed here is that of Kern.[6] Avoiding the derivation of the similarity solution, the final result is written in terms of a convective component, a diffusion component, and a conductive component, as follows:

$$h_{conv} (T_g - T_c) + K_g M_v h_{fg} (P_v - P_c) = h_{cond} (T_c - T_w). \qquad (28)$$

The first term on the left of Eq. (28) is the convective heat transfer component, where h_{conv} is given by the usual Nusselt correlation for convective heat transfer between a hot gas and a cooled vertical wall. The second term is the diffusive heat transfer component, where M_v is the vapor molecular weight, h_{fg} is the latent heat of vaporization, and K_g is the diffusion coefficient which incorporates the similarity assumptions. The overall diffusion coefficient is given by,

$$K_g = \frac{h_{conv} (C_p \mu / k)^{2/3}}{C_p P_{fg} M_n (\mu / \rho k_g)^{2/3}} \qquad (29)$$

In Eq. (29) the Prandtl number grouping, $C_p\mu/k$, and the Schmidt number grouping, $\mu/\rho k_g$, are immediately recognized, while M_m is a mean molecular weight of gas and vapor, and p_{fg} is the log-mean sodium vapor pressure across the diffusion region. The term on the right of Eq. (28) represents the conductive heat flux through the liquid sodium film. For the effective heat transfer coefficient,

$$h_{cond} = \frac{K}{\delta} ,$$

the Nusselt correlation for condensation given in Eq. (27) should be used.

Due to the relatively low thermal conductivity of water, a significant temperature differential may occur between the wall and the film surface. For condensation of steam, therefore, it is necessary to assume an interface temperature, T_c; use the saturation curve to calculate the vapor pressure, P_c, at the interface; calculate the three components of Eq. (28) and iterate on T_c until the equation is balanced. The high thermal conductivity of liquid sodium, however, makes this iterative process unnecessary for sodium vapor condensation. The temperature differential across the film rarely exceeds $1^{o}K$ in most situations, so that with little loss of accuracy the interface temperature in the two terms on the left of Eq. (28) may be taken as the wall temperature, T_w. The vapor mass flux at the interface is then found simply by dividing the diffusion component of Eq. (28) by the latent heat to get,

$$G_v = K_g M_v (P_v - P_c). \qquad (30)$$

To calculate the total reflux rate, it is only necessary to add the components from the various heat structure surfaces,

$$\dot{m}_{v\ell} = \sum_i G_i A_i . \qquad (31)$$

The interface temperature approximation discussed previously is justified by the results shown in Figures 18 and 19. These figures show the film temperature differential, $(T_i - T_w)$, as a function of the temperature difference

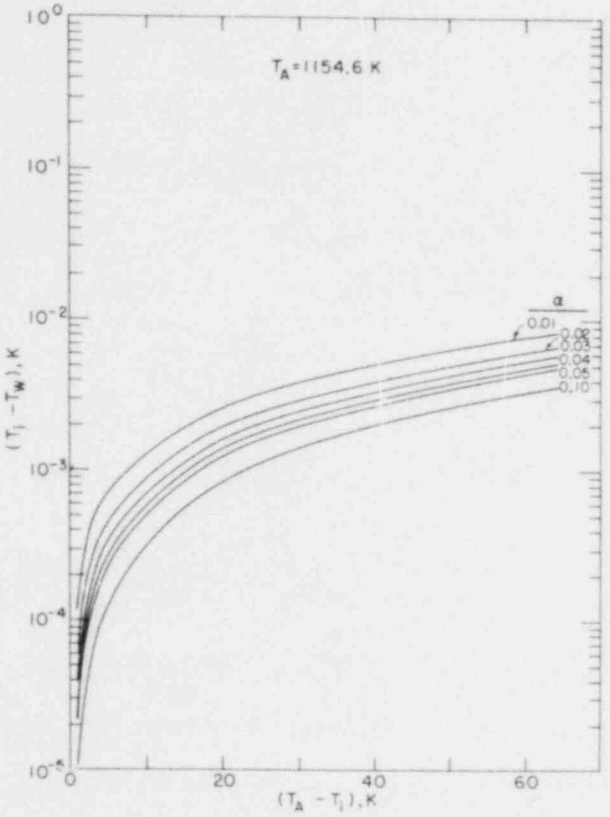

Figure 18. Temperature Drop Across the Sodium Film

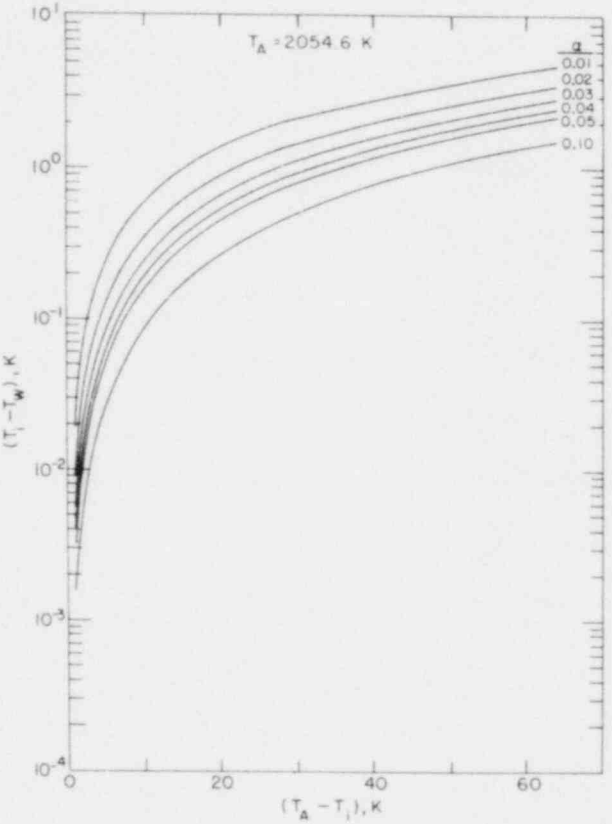

Figure 19. Temperature Drop Across the Sodium Film

between the atmosphere and the wall, (T_A-T_i), and the mass fraction of non-condensables, α. Figure 18 is the result of an atmospheric temperature equal to the sodium boiling temperature at 1 atm. Figure 19 is for an atmospheric temperature 900°K above the 1 atm boiling temperature. At the sodium boiling temperature, the maximum temperature differential in the film was only 0.01°K even for very low gas concentration and high convective heat transfer rates. At the higher temperature in Figure 19, a differential temperature of 5°K was approached, but only at the unrealistic condition in which low non-condensable concentrations were artificially combined with high convective heat transfer components. These two parameters are actually not independent, so that the lower the gas concentration the lower will be the convective component.

The effect of non-condensables on the heat flux (and thus the condensation rate) is shown in Figure 20. The heat flux ratio given on the ordinate in Figure 20 is simply the ratio of the heat flux in the presence of non-condensables to the heat flux in the absence of non-condensables. The trends seen in Figure 20 are expected; the heat flux ratio increasing with decreasing gas fraction and increasing temperature differential. It should be noted that with a sufficiently high temperature difference between the gas and the wall, the heat flux ratio can exceed 1.0. This is due to the convective component which does not exist in the absence of non-condensables. However, the ratio of the sodium condensation rate with non-condensables to the condensation rate without non-condensables can not exceed 1.0, regardless of the magnitude of the convective heat transfer component.

The evaporation model employs the standard solutions for mass transfer by convectively enchanced diffusion. The problem is basically the diffusion of sodium vapor from the pool surface at sodium vapor mass fraction $m_{1,s}$ to the

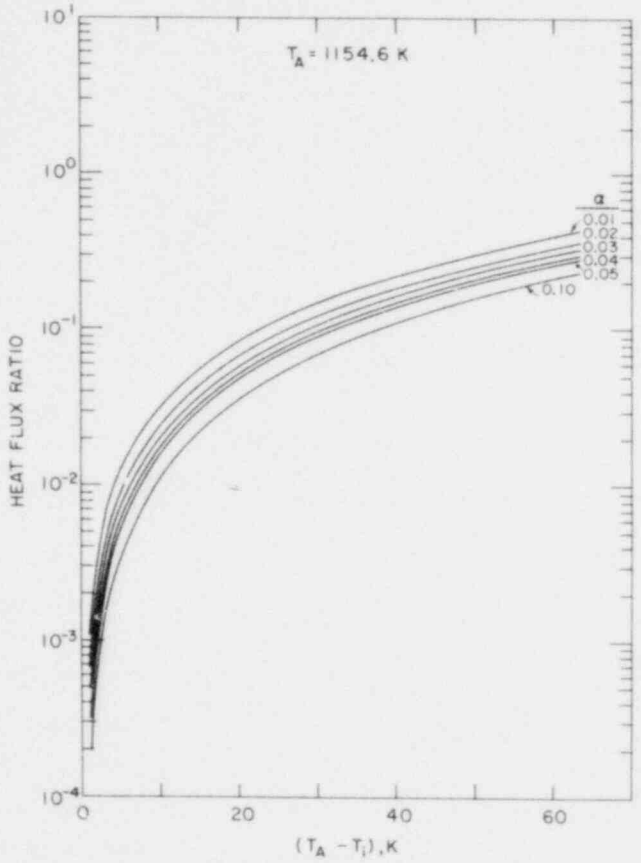

Figure 20. Ratio of Heat Flux in the Presence of Non-Condensibles to the Heat Flux without Non-Condensibles

cell atmosphere at a mass fraction $m_{l,e}$. The Nusselt number correlations for laminar and turbulent convection yield:

Laminar

$$G_{evap} = 0.54 \frac{\rho D_{12}}{L} (m_{l,s} - m_{l,e}) (GrSc)^{1/4} \tag{32}$$

Turbulent

$$G_{evap} = 0.12 \frac{\rho D_{12}}{L} (m_{l,s} - m_{l,e}) (GrSc)^{1/3} \tag{33}$$

Here, G_{evap} is the evaporation flux, Sc is the Schmidt Number, and D_{12} is the diffusion coefficient for sodium vapor through nitrogen gas. The Schmidt Number is defined by:

$$S_c = \frac{\mu}{\rho D_{12}} . \tag{34}$$

The viscosity, μ, and the diffusion coefficient D_{12}, were calculated using the Lennard-Jones potential in the Chapman-Enskog kinetic theory of gases[7]:

$$\mu = 4.158 \times 10^{-8} \frac{\sqrt{MT}}{\sigma^2 \Omega_\mu} , \tag{35}$$

$$D_{12} = 8.283 \times 10^{-7} \frac{\sqrt{T^3 \left[\frac{1}{M_{Na}} + \frac{1}{M_{N2}}\right]}}{\sigma_{12}^2 \Omega_D P} . \tag{36}$$

The collision integral Ω_μ, and the collision integral for mass transfer Ω_D, which are given in tabular form as a function of temperature, were curve fit for use in CONAN. The Lennard-Jones parameter σ_{12} is simply the average of the parameters for sodium vapor and nitrogen:

$$\sigma_{12} = \frac{1}{2}(\sigma_{Na} + \sigma_{N2}) . \tag{37}$$

The total evaporation rate is arrived at by multiplying the evaporation mass flux in Equation 32 or 33 by the pool area:

$$\dot{m}_{evap} = A_{p\ell} G_{evap} \tag{38}$$

VII. EFFECTS OF CONDENSATION AND EVAPORATION

A number of cases were run using the CONAN code in an effort to determine the effect of condensation on the containment transient. In order to accomplish this, it was necessary to model the containment in more detail than was needed in the previous sensitivity and comparison studies. This was accomplished by more accurately modeling the heat structures in the reactor cavity, including the appropriate steel masses and the heat sinks available in the surrounding concrete. In addition, the concrete floor of the reactor containment building was included. Four separate heat structures were used in the reactor cavity; these included the concrete and firebrick structure beneath the hot liner, the concrete behind the cold liner, the submerged vessel insulation, and the non-submerged vessel insulation. Similarly, the heat sinks were modeled to include the submerged liner (hot liner), the non-submerged liner (cold liner), the submerged part of the reactor vessel, and the non-submerged part of the reactor vessel (including the vessel head).

The first case (Case 004) considered in the present sequence was run with the above configuration, but did not include condensation or evaporation. Case 005, which is the second case in this sequence, incorporated condensation but not evaporation. The third case (006) modeled both condensation and evaporation. The RCB pressure transients for these three cases are shown in Figure 21. The obvious result is that for cases 005 and 006 the pressure transient is largely mitigated by the condensation process, whereas for Case 004 in which

condensation was neglected, the pressure transient was considerably more severe, reaching over 0.18 MP_a.

To interpret these results, it is necessary to describe in a little more detail how the condensation and evaporation models are meshed with the CONAN overall modeling. For Case 005, in which only condensation was considered, the "saturated atmosphere" model discussed previously was used exclusively. That is, the atmosphere was assumed to be saturated with sodium vapor corresponding to the pool temperature. The rate of condensation on the above-pool structures, together with the mass loss by venting, was assumed to be exactly balanced by sodium vaporized from the pool, whether that be by evaporation or by bulk boiling. These assumptions are probably not conservative in that they overestimate the sodium vapor concentration in the atmosphere. This results in an overprediction of the condensation rate, and thus the reflux rate. This effect is clearly evident in Figure 22. Whereas boiling (1155°K) is obtained in about 22 hours in the absence of condensation, the pool temperature for the case with condensation did not quite reach 1100°K at 100 hours, and, judging from the slope of the curve at 100 hours, would probably not reach incipient boiling before 400 to 500 hours. These results, therefore, pointed out the necessity of incorporating a more realistic pre-boiling evaporation model.

The overall modeling was altered in order to incorporate the evaporation model. To accomplish this, it was required that the sodium vapor mass be included as one of the unknowns and a mass balance be written on it. Formerly the sodium vapor mass was a known function of the pool and the atmospheric temperatures. The calculations were then separated into three phases, a pre-boiling phase, a pre-saturation phase, and finally a full boiling phase. In the pre-boiling phase the sodium vapor mass was determined by the following mass-balance equation:

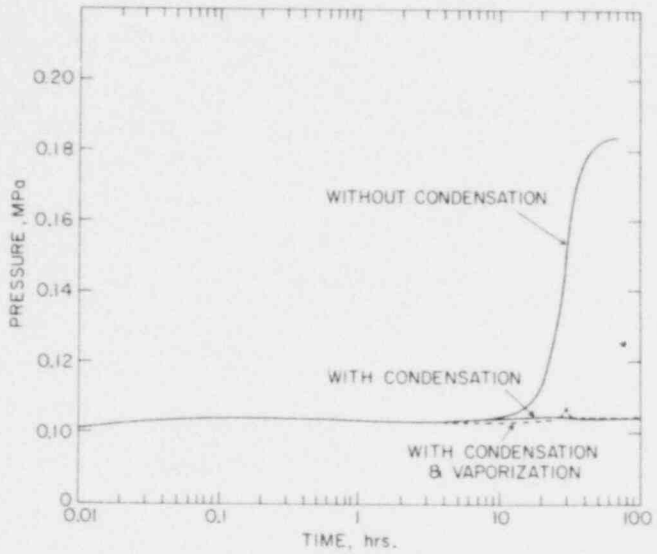

Figure 21. Effects of Condensation and Evaporation on the RCB Pressure Transient

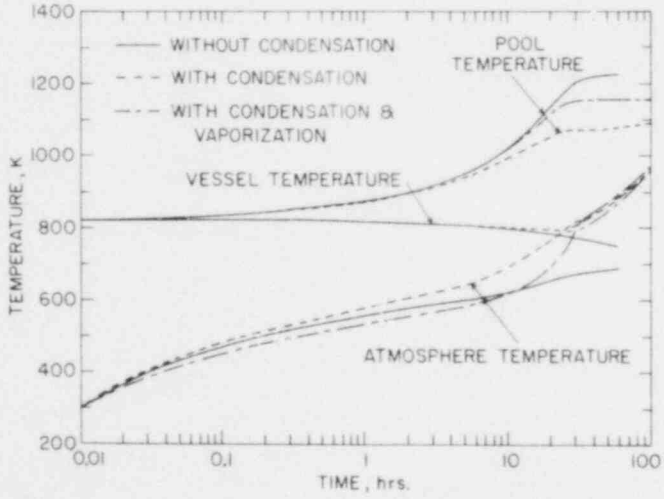

Figure 22. Effects of Condensation on the Cavity Temperatures

$$\frac{dm_{sv}}{dt} = \dot{m}_{evap} - \dot{m}_{cond} - \dot{m}_{vent}, \tag{39}$$

where $\dot{m}_{sv}$ is the sodium vapor mass, $\dot{m}_{evap}$ is the evaporation rate, $\dot{m}_{cond}$ is the condensation rate, and $\dot{m}_{vent}$ is the sodium vapor venting rate. In the second phase, which begins when the pool reaches incipient boiling, the pool temperature remains constant at the boiling temperature and the first term on the right side of Eq. (39), $\dot{m}_{evap}$, is replaced by the boiling rate term, $\dot{m}_{boil}$. The vaporization rate is calculated by assuming that, until the atmosphere reaches saturation, the pool temperature remains constant and all the decay heat that exceeds the pool heat losses is directed into vaporizing sodium, so that:

$$\dot{m}_{boil} = \frac{\left[Q_D - \sum_i A_i h_i (T_p - T_i)\right]}{h_{fg}} . \tag{40}$$

In the third phase or the full boiling phase, the saturated atmosphere condition is reestablished and the transient proceeds as before.

The results of the case in which both condensation and evaporation are considered is also shown in Figure 22. It is clearly seen that the reflux rate is controlled and limited by the evaporation rates. The reflux rate, being thus limited, results in a more realistic pool temperature transient in which incipient boiling is reached at about 30 hours. However, even though the boiling temperature is reached much earlier than for the case in which evaporation was neglected, an immediate containment pressure transient is not forthcoming. The reason for this can be seen in Figures 23 and 24, which show the condensation vs. evaporation for Case 006, and the sodium vapor density for all three cases, respectively. Figure 23 indicates that within about 5 hours the condensation and evaporation rate are very nearly balanced. Even at 30 hours, when boiling replaces evaporation as the sodium vapor source, the condensation rate quickly

adjusts and balances the vaporization rate. After incipient boiling, as shown in Figure 22, the vessel steel temperature rises rapidly due to enhanced condensation heat transfer, and the condensation rate begins to fall off. Figure 24 shows that, although the sodium vapor density starts at zero for Case 006, and is considerably below the other two cases in the pre-boiling phase, it ultimately attains the same value in the second phase as was obtained for Case 005.

What is evidently implied in these results, although Case 006 has not been run out past 100 hours, is that although the pool reaches boiling fairly early in the accident sequence, condensation will continue to keep abreast of vaporization until the structures above the pool are elevated to nearly the pool temperature, at which time the cavity will begin to pressurize, forcing sodium vapor into the reactor containment building and generating the combustion-driven pressure transient seen in previous cases. The final effect of condensation, therefore, is that the containment building transient is effectively delayed until the structures in the cavity above the pool are brought into thermal equilibrium with the pool. At that point, the transient will proceed with a sodium vapor transport rate into the RCB which conforms to an effective configuration in which all the structures contained in the reactor cavity are in thermal equilibrium with the pool and being heated at approximately the same rate.

VIII. CONCLUSIONS AND PROJECTIONS FOR FURTHER ANALYSIS

A number of modeling differences exist between the CACECO and CONAN codes. The primary differences concern the assumption of thermal equilibrium between the cell atmosphere and the sodium pool, and the treatment of condensation and vaporization. Ironically, the two models have a similar effect in terms of containment building pressurization. The thermal equilibrium model

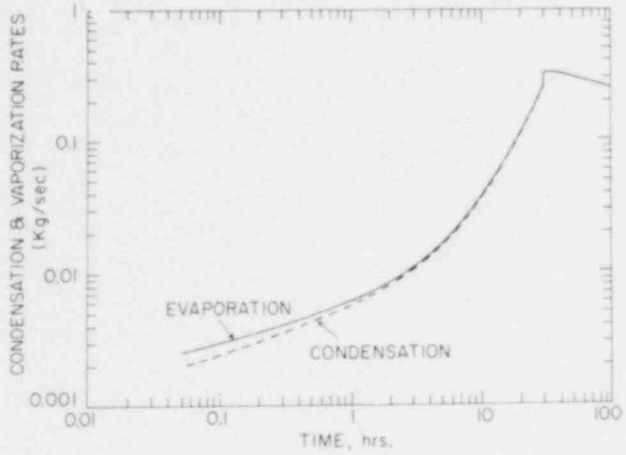

Figure 23. Condensation versus Evaporation Rates

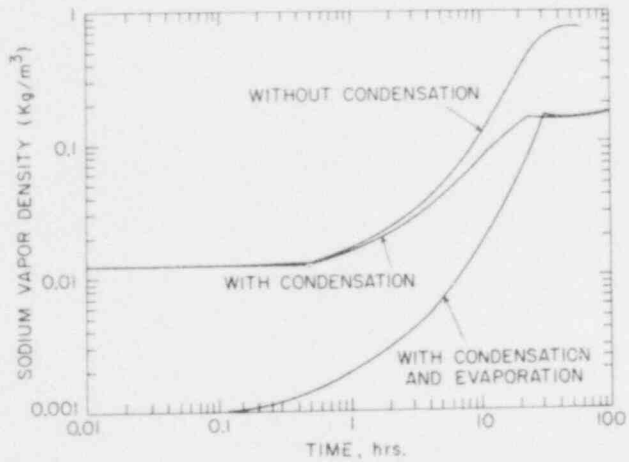

Figure 24. Effects of Condensation and Evaporation on Sodium Vapor Density

delays pressurization by making it necessary to bring the vessel and other cavity structures to the incipient sodium boiling temperature before boiling and pressurization can occur. In addition, it creates high heat transfer rates since the structures and walls in the cavity essentially "see" the pool temperatures even though they do not actually contact the pool. On the other hand, the mechanistic treatment of condensation also results in delaying containment pressurization. This occurs as a result of the balance between the bulk boiling rate and the condensation of sodium vapor on the steel structures above the pool. Although condensation in the pre-boiling phase does not have a significant effect on the time required to bring the pool to boiling, the enhanced condensation rates subsequent to incipient boiling apparently can keep up with the sodium vaporization rate during boiling as long as the above-pool-structures are cooler than the pool. Since condensation can remove sodium vapor as fast as the decay heat can vaporize it, the pressure in the cavity is not immediately elevated and the containment transient is effectively delayed until the cavity structures are sufficiently heated.

The CACECO code treatment of condensation and evaporization are non-mechanistic and tend to overpredict the reflux rate and retard the time of incipient boiling.

When condensation and evaporation are incorporated into the CONAN code, a discontinuity occurs at the point of incipient boiling. Because the dynamics of the boiling process are too complicated to model mechanistically in the present code, this discontinuity between the pre-boiling and boiling phases is difficult to remove. Future work should attempt to address this problem. Follow-on work with the CONAN code should also include treatment of the possible presence of water vapor, hydrogen, and carbon dioxide, as well as a model for the chemical and thermal effects of the sodium-concrete reaction.

Inspection of the sodium vapor pressure for Case 006 shows that the atmosphere above the pool is supersaturated. However, condensation of sodium vapor on aerosols or dust particles will have purged these from the atmosphere fairly early in the sequence, with the result that nucleation sights will probably not be available and a supersaturated condition could be maintained. Cloud chamber experiments with various types of vapors have shown that vapor pressures nearly two orders of magnitude above saturation are possible before homogeneous nucleation occurs. Post-accident conditions in the reactor cavity, namely, a heated sodium pool with a large heat sink in the atmosphere above it, supply the condition for a high degree of supersaturation. Thus, future work might entail determining the degree of supersaturation at various conditions for sodium vapor in nitrogen gas, and incorporating a homogeneous nucleation model into the code for determination of sodium rain-out and the reflux rate due to this phenomena.

REFERENCES

1. S.S. Tsai, R.D. Gasser, W.T. Pratt, "Containment Design Basis Accident for LMFBRs: Review of Methods," BNL-NUREG-23221, (September 1977).
2. G.H. Golden et al., "Thermophysical Properties of Sodium," ANL-7323, (August 1967)
3. "Containment Margins in FFTF for Postulated Failure of In-Vessel Post-Accident Heat Removal," HEDL-TME 77-18, (April 1977).
4. E.M. Sparrow, S.H. Lin, "Condensation in the Presence of a Non-condensable Gas," J. Heat Transfer, Trans. ASME, C86:430, 1963.
5. N.H. McAdams, Heat Transmission, (McGraw-Hill Book Co., New York, 1954), 3rd ed., Chapter 13, p. 355.
6. P.Q. Kern, Process Heat Transfer, (McGraw-Hill Book Co., New York, 1950), Chapter 12, p. 252.
7. D.K. Edwards et al., "Transfer Processes," (Holt, Rinehart & Winston, Inc., New York, 1973), Chap. 7, p. 206-212.

NOMENCLATURE

A_{12} - Cross-Section flow area between cells 1 and 2.

A_i - Surface area of ith heat structure.

A_{pl} - Surface area of sodium pool in cell 1.

A_{pw} - Area of wall contacting the pool.

A_R - Coefficient in sodium gas constant regression.

A_S - Coefficient in sodium vapor pressure correlations.

A_{W1} - Area of wall contacting cell 1 atmosphere.

A_{W2} - Area of wall contacting cell 2 atmosphere.

B_R - Coefficient in sodium gas constant regression.

B_S - Coefficient in sodium vapor pressure correlations.

C_{12} - Nozzle flow coefficient for flow from cell 1 to 2.

C_P - Constant pressure heat capacity.

C_R - Coefficient in sodium gas constant regression.

C_S - Coefficient in sodium vapor pressure correlation.

C_V - Constant volume heat capacity.

D_{12} - Diffusion Coefficient.

G_{evap} - Evaporation Flux.

G_i - Sodium vapor condensation mass flux to the ith structure.

Gr - Grashof Number.

G_V - Sodium vapor condensation mass flux.

g - Acceleration due to gravity.

h_e - Enthalpy of material entering the control volume.

h_i - Heat transfer coefficient to the ith heat structure.

h_ℓ - Enthalpy of material leaving the control volume.

h_{comb} - Heat of combustion for sodium vapor.

h_{cond} - Effective heat transfer coefficient due to conduction through the vapor film.

h_{conv} - Convective heat transfer coefficient.

h_{fg} - Latent heat of vaporization for sodium.

h_{N1} - Enthalpy of nitrogen in Cell 1.

h_{N2} - Enthalpy of nitrogen in Cell 2.

h_{O2} - Enthalpy of oxygen in Cell 2.

h_{P1} - Heat transfer coefficient between the pool surface and the Cell 1 atmosphere.

h_{PW} - Heat transfer coefficient between the pool and the wall.

h_{SV1} - Enthalpy of sodium vapor in Cell 1.

h_{SVP} - Enthalpy of sodium vapor at the pool temperature.

h_{W1} - Heat transfer coefficient between the atmosphere and the wall in Cell 1.

h_{W2} - Heat transfer coefficient between the atmosphere and the wall in Cell 2.

K_g - Sodium overall similarity diffusion coefficient.

k - Thermal conductivity.

k_g - Diffusion coefficient for sodium vapor through nitrogen gas.

L - Characteristic length.

M - Total mass of gas in the system.

M_m - Mean molecular weight of gas and vapor.

M_{Na} - Molecular weight of sodium.

M_{N2} - Molecular weight of nitrogen.

m - Gas mass.

m_1 - Gas mass in Cell 1.

$m_{1,e}$ - Mass fraction in atmosphere.

$m_{1,s}$ - Mass fraction at pool surface.

m_2 - Gas mass in Cell 2.

m_{10} - Initial mass of gas in Cell 1.

m_{20} - Initial mass of gas in Cell 2.

m_e - Mass of gas entering the system.

m_ℓ - Mass of gas leaving the system.

m_{N1} - Mass of nitrogen in Cell 1.

m_{N2} - Mass of nitrogen in Cell 2.

m_{O2} - Mass of oxygen in Cell 2.

m_{NO1} - Mass of Na_2O in Cell 1.

m_{NO2} - Mass of Na_2O in Cell 2.

$\dot{m}_p$ - Mass of sodium pool.

$\dot{m}_{s1}$ - Mass of sodium vapor in Cell 1.

$\dot{m}_{sv}$ - Mass of sodium vapor.

$\dot{m}_{boil}$ - Sodium boiloff rate.

$\dot{m}_{cond}$ - Sodium vapor condensation rate.

$\dot{m}_{evap}$ - Sodium evaporation rate.

$\dot{m}_{12}$ - Mass flowrate from Cell 1 to Cell 2.

$\dot{m}_{21}$ - Mass flowrate from Cell 2 to Cell 1.

$\dot{m}_{N12}$ - Mass flowrate of nitrogen from Cell 1 to Cell 2.

$\dot{m}_{N21}$ - Mass flowrate of nitrogen from Cell 2 to Cell 1.

$\dot{m}_{N23}$ - Mass flowrate of nitrogen from Cell 2 to outside.

$\dot{m}_{O21}$ - Mass flowrate of oxygen from Cell 2 to Cell 1.

$\dot{m}_{O23}$ - Mass flowrate of oxygen from Cell 2 to outside.

$\dot{m}_{Ocomb}$ - Oxygen combustion rate.

$\dot{m}_{s12}$ - Mass flowrate of sodium vapor from Cell 1 to Cell 2.

$\dot{m}_{scomb}$ - Sodium combustion rate.

$\dot{m}_{vent}$ - Sodium vapor venting rate.

$\dot{m}_{vL}$ - Sodium condensation rate.

P_1 - Cell 1 pressure.

P_2 - Cell 2 pressure.

P_{10} - Cell 1 initial pressure.

P_{20} - Cell 2 initial pressure.

P_c - Interfacial sodium vapor pressure.

P_v - Sodium vapor pressure.

P_{equil} - Equilibrium pressure.

P_{fg} - Log mean of the noncondensable gas pressure near the interface.

P_{N1} - Nitrogen partial pressure in Cell 1.

P_{N2} - Nitrogen partial pressure in Cell 2.

P_{O2} - Oxygen partial pressure in Cell 2.

P_{sat} - Sodium saturation pressure.

P_{s1} - Sodium vapor pressure in Cell 1.

Q_D - Decay heat rate.

Q - Heat loss rate.

R - Universal gas constant.

R_{comb} - Combustion rate.

R_N - Effective gas constant for nitrogen.

R_O - Effective gas constant for oxygen.

Sc - Schmidt Number.

T - Temperature.

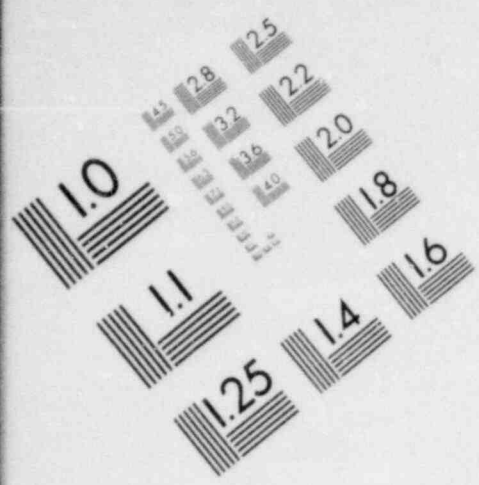

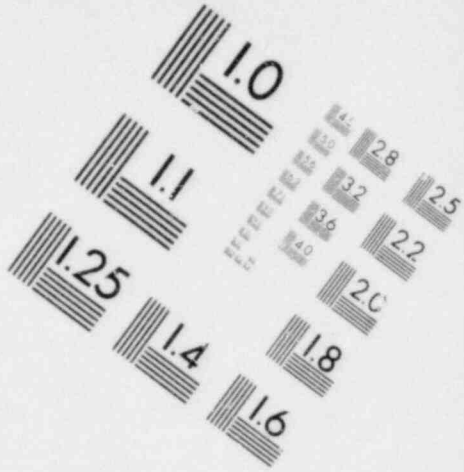

IMAGE EVALUATION
TEST TARGET (MT-3)

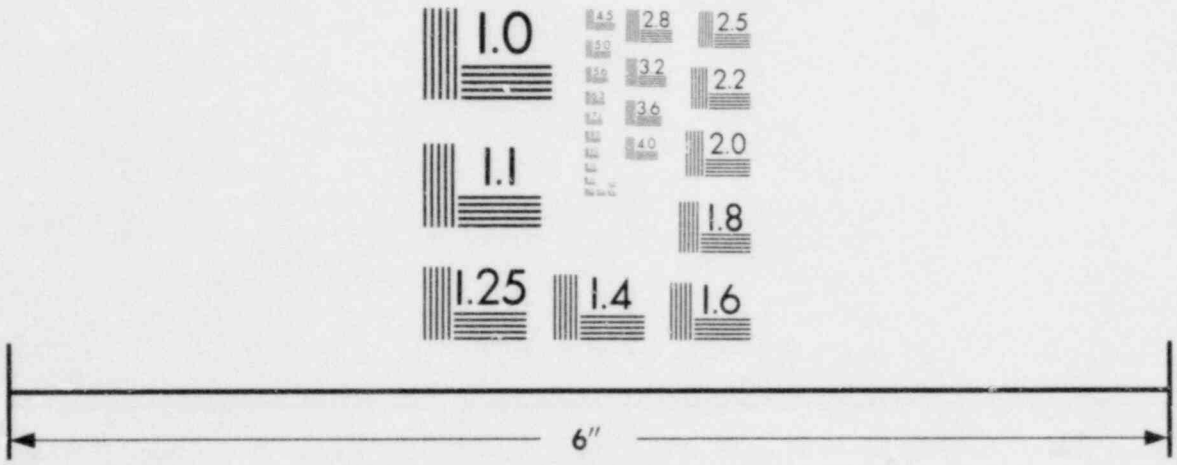

MICROCOPY RESOLUTION TEST CHART

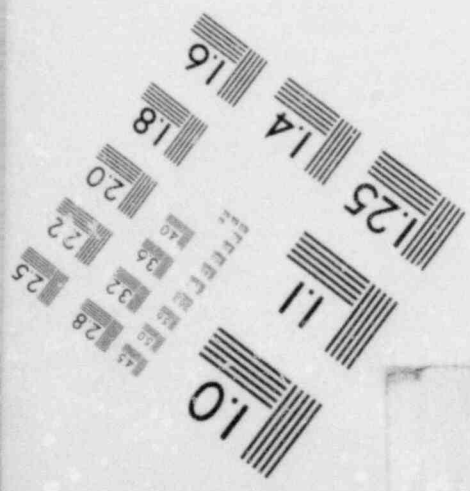

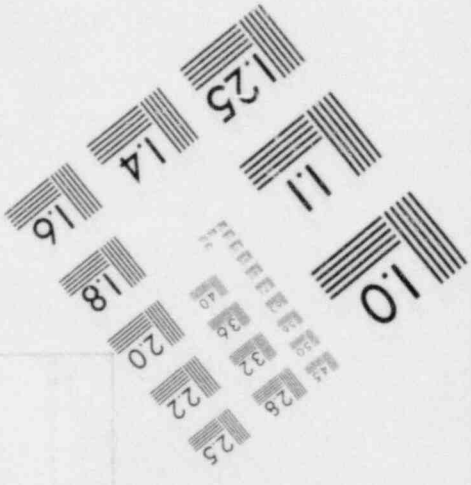

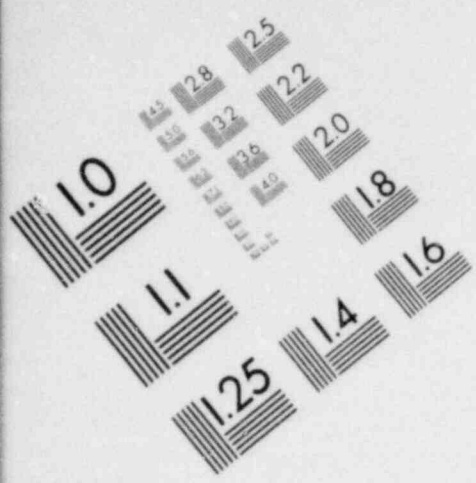

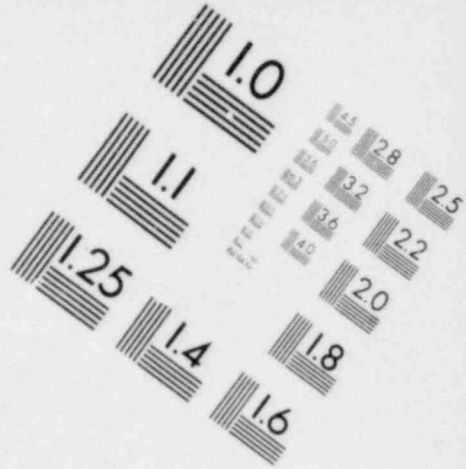

IMAGE EVALUATION
TEST TARGET (MT-3)

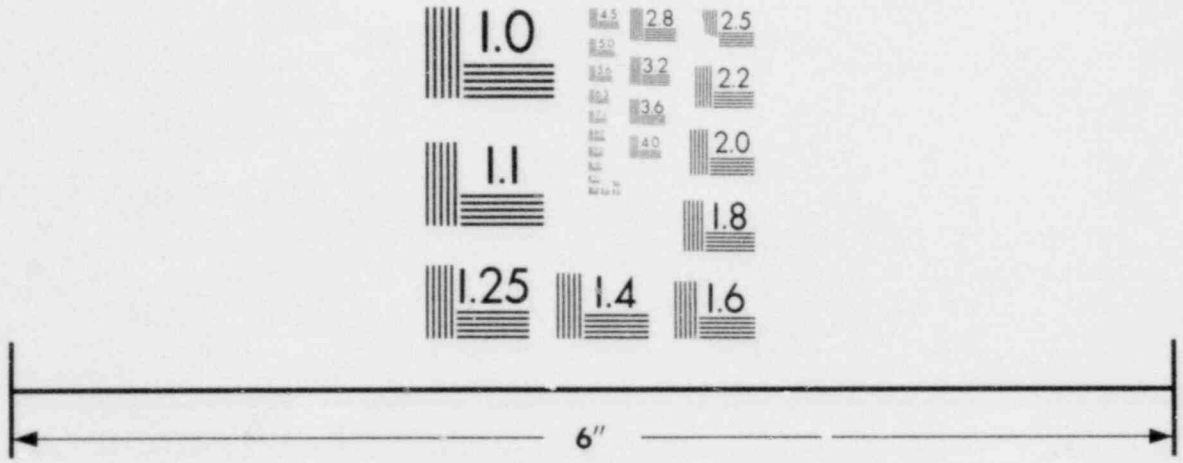

MICROCOPY RESOLUTION TEST CHART

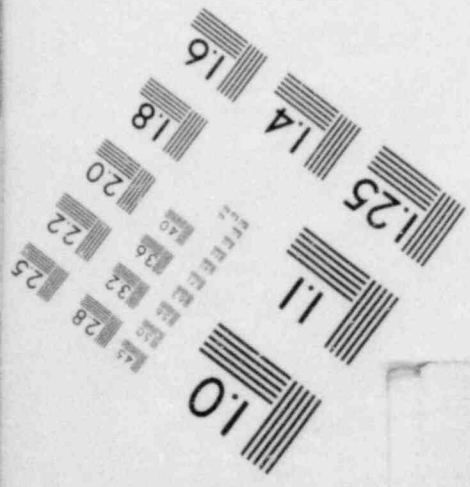

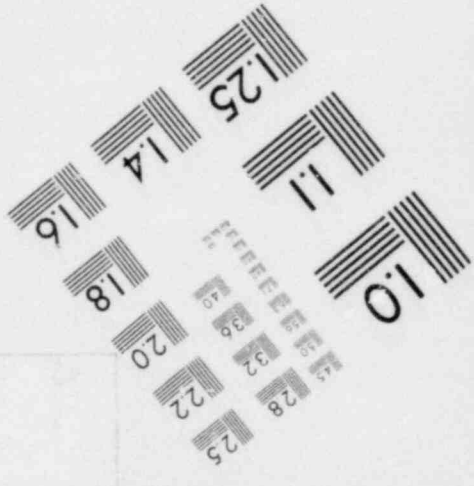

T_1 - Temperature in Cell 1.

T_2 - Temperature in Cell 2.

T_{10} - Initial temperature in Cell 1.

T_{20} - Initial temperature in Cell 2.

T_c - Interface temperature.

T_i - Interface temperature.

T_g - Gas temperature.

T_p - Pool temperature.

T_s - Interface temperature.

T_w - Wall temperature.

T_{pw} - Temperature of the wall adjacent to the pool.

T_{w1} - Temperature of the wall in Cell 1.

T_{w2} - Temperature of the wall in Cell 2.

T_{wi} - Surface temperature of the ith structure.

t - Time

u - Internal energy.

u_{N1} - Internal energy of nitrogen in Cell 1.

u_{N2} - Internal energy of nitrogen in Cell 2.

u_{NO1} - Internal energy of Na_2O in Cell 1.

u_{NO2} - Internal energy of Na_2O in Cell 2.

u_{O2} - Internal energy of oxygen in Cell 2.

u_{slp} - Internal energy of liquid sodium.

u_{sv1} - Internal energy of sodium vapor in Cell 1.

V_1 - Cell 1 volume.

V_2 - Cell 2 volume.

Z - Vertical coordinate.

α - Mass fraction of noncondensable gases.

γ - Ratio of constant pressure to constant volume heat capacities.

δ - Sodium film thickness.

μ - Viscosity

ρ_1 - Total density of Cell 1 atmosphere.

ρ_2 - Total density of Cell 2 atmosphere.

ρ_ℓ - Liquid sodium density.

ρ_v - Sodium vapor density.

σ - Lennard-Jones parameter.

Ω_D - Collision integral for diffusion.

Ω_μ - Collision integral for viscosity.

REPORT DISTRIBUTION

Mr. Harry Alter, Chief (1)
Safety Analysis Branch
Division of Reactor Development
and Demonstration
Department of Energy
Washington, D. C. 20545

Assistant Director for Reactor (1)
Safety
Division of Reactor Development
and Demonstration
Department of Energy
Washington, D. C. 20545

Dr. Raymond Alcouffe (1)
Los Alamos Scientific Laboratory
Mail Stop 269
P. O. Box 1663
Los Alamos, N. M. 87545

Dr. Robert Avery, Director (2)
Reactor Analysis & Safety
Division
Argonne National Laboratory
9700 South Cass Avenue
Argonne, Illinois 60439

Dr. L. W. Caffey, Director (1)
CRBR Plant Project Office
Department of Energy
P. O. Box U
Oak Ridge, Tennessee 37830

Dr. R. Curtis, Chief (1)
Analytical Advanced Reactor
Safety Research Branch
Nuclear Regulatory Commission
Washington, D. C. 20555

Dr. William Davey (1)
Q Division Leader
Mail Stop 561
Los Alamos Scientific Laboratory
P. O. Box 1663
Los Alamos, N. M. 87545

Dr. Carl A. Erdman (1)
Department of Nuclear Engineering
University of Virginia, Thornton Hall
Charlottesville, Virginia 22901

Dr. R. Ferguson, Director (1)
Fast Flux Test Facility Project Office
Department of Energy
P. O. Box 550
Richland, Washington 99352

Mr. Domenic Vassallo, Acting Director (1)
Division of Project Management
Nuclear Regulatory Commission
Washington, D. C. 20555

Mrs. H. Gearin, Licensing (1)
Assistant for Special Projects
Division of Project Management
Nuclear Regulatory Commission
Washington, D. C. 20555

Mr. C. R. Hahn, Manager (1)
Fuels Design and Development
Pacific Northwest Laboratories
P. O. Box 999
Richland, Washington 99352

Dr. Stephen H. Hanauer (1)
Technical Advisor
Office of the Executive Director
for Operations
Nuclear Regulatory Commission
Washington, D. C. 20555

Mr. K. Hikido, Manager (1)
General Electric Company
Systems Evaluation & Safety
Engineering
Fast Breeder Reactor Department
310 DeGuigne Drive
Sunnyvale, California 94086

Dr. Harry Hummel (1)
Applied Physics Division
Argonne National Laboratory
Building 208
9700 South Cass Avenue
Argonne, Illinois 60439

Dr. Vijen Javeri (1)
Fast Reactor Accident Analysis
Gesellschaft fur Reaktorsicherheit
(GRS) mbH
Glockengasse 2·5000 Koln 1
West Germany

Dr. William Kastenberg (1)
Department of Chemical Nuclear
and Thermal Engineering
University of California
at Los Angeles
Los Angeles, California 90024

Dr. C. N. Kelber, Assistant Director (2)
for Advanced Reactor Safety Research
Division of Reactor Safety Research
Nuclear Regulatory Commission
Washington, D. C. 20555

Mr. Richard Lorenz (1)
Air/Ground Explosions Division
Naval Surface Weapons Center
White Oak
Silver Spring, Maryland 20910

Dr. Roger J. Mattson, Director (1)
Division of Systems Safety
Office of Nuclear Reactor Regulation
Nuclear Regulatory Commission
Washington, D. C. 20555

Dr. James F. Meyer (15)
Advanced Reactors Branch
Division of Project Management
Nuclear Regulatory Commission
Washington, D. C. 20555

Professor F. J. Munno (1)
Nuclear Engineering Program
Department of Chemical
Engineering
University of Maryland
College Park, Maryland 20745

Dr. David Okrent (1)
Department of Chemical Nuclear and
Thermal Engineering
University of California
at Los Angeles
Los Angeles, California 90024

Mr. Frank E. Panisko, Senior (1)
Development Engineer
Fuels Design and Development
Pacific Northwest Laboratories
P. O. Box 999
Richland, Washington 99352

Mr. D. F. Ross, Assistant Director (1)
for Reactor Safety
Nuclear Regulatory Commission
Washington, D. C. 20555

Secretary, Advisory Committee on (5)
Reactor Safeguards
Nuclear Regulatory Commission
Washington, D. C. 20555

Dr. Arkal S. Shenoy, Manager (1)
Systems & Safety Analysis
Branch
Gas Cooled Fast Breeder Reactor
General Atomic Company
P. O. Box 81608
San Diego, California 92138

Mr. M. Silberberg, Chief (1)
Experimental Fast Reactor
Safety Research Branch
Division of Reactor Safety Research
Nuclear Regulatory Commission
Washington, D. C. 20555

Mr. Daniel E. Simpson (1)
Manager, Safety Engineering
Hanford Engineering Development
Laboratory
P. O. Box 1970
Richland, Washington 99352

Dr. Themis P. Speis, Chief (1)
Advanced Reactors Branch
Division of Project Management
Nuclear Regulatory Commission
Washington, D. C. 20555

Dr. Michael Stevenson (2)
Los Alamos Scientific Laboratory
P. O. Box 1663
Los Alamos, N. M. 87545

Dr. David Swanson (1)
Materials Sciences Laboratory
Aerospace Corporation
P. O. Box 92957
Los Angeles, California 90009

Technical Information Center (1)
Nuclear Regulatory Commission
P. O. Box 62
Oak Ridge, Tennessee 37830

Dr. Theo G. Theofanous (1)
132 Pathway Lane
Lafayette, Indiana 47906

U. S. Nuclear Regulatory Commission (1)
Division of Technical Information
and Control
7920 Norfolk Avenue
Bethesda, Maryland 20014

Dr. J. V. Walker, Dept. Manager (1)
Reactor Research and Development
Sandia Laboratories
P. O. Box 5800
Albuquerque, N. M. 87115

BNL Distribution

DNE Chairman (1)

RSP Associate Chairman (1)

RSP Division Heads (5)

SEG/E&ARS Division (8)

BNL Reactor Safety Library (2)